

Extended weakly nonlinear theory of planar nematic convection

Emmanuel Plaut* and Werner Pesch

Physikalisches Institut der Universität Bayreuth, 95440 Bayreuth, Germany

(Received: 13 May 1998)

We study theoretically convection phenomena in a laterally extended planar nematic layer driven by an ac-electric field (electroconvection in the conduction regime) or by a thermal gradient (thermoconvection). We use an order-parameter approach and demonstrate that the sequence of bifurcations found experimentally or in the numerical computations can be recovered, provided a homogeneous twist mode of the director is considered as a new active mode. Thus we elucidate the bifurcation to the new “abnormal rolls” [E. Plaut *et al.*, Phys. Rev. Lett. **79**, 2367 (1997)]. The coupling between spatial modulations of the twist mode and the mean flow is shown to give an important mechanism for the long-wavelength zig-zag instability. The twist mode is also responsible for the widely observed bimodal instability of rolls. Finally, a Hopf bifurcation in the resulting bimodal structures is found, which consists of director oscillations coupled with a periodic switching between the two roll amplitudes. A systematic investigation of the *microscopic* mechanisms controlling all these bifurcations is presented. This establishes a close analogy between electroconvection and thermoconvection. Moreover, a “director-wave-vector frustration” is found to explain most of the bifurcations. [S1063-651X(99)01102-2]

PACS number(s): 47.20.Ky, 47.20.Bp, 42.70.Df

I. INTRODUCTION

The rich variety of instabilities in nematic liquid crystals has always attracted great interest among experimentalists and theorists [1–3]. Nematic liquid crystals are fluids which show a long-range uniaxial ordering in the orientation of their rodlike molecules. The average orientation defines the director field \mathbf{n} , which is also the local anisotropy axis of the medium. Due to the coupling of \mathbf{n} to the other fields of the fluid (velocity, temperature, etc.), specific *focusing mechanisms* lead to new convective instabilities [4,5]. In the planar setup used by most researchers, a nematic layer is sandwiched between two horizontal plates, where the director is fixed in a horizontal direction $\hat{\mathbf{x}}$ (planar anchoring). Since the rotational symmetry in the layer plane is broken, this system has become a prime example for anisotropic convection [3,6].

Two realizations of convection in a planar nematic layer exist. Under the application of a vertical (along z) ac-electric field of angular frequency ω , *charge focusing* [4,7] leads to electroconvection (EC). Thin cells of thickness $d \approx 10\text{--}100 \mu\text{m}$ can be used. Consequently the characteristic times are small and very large aspect ratios (cell width/ d) can be obtained; also for these reasons EC has been extensively studied [6]. Alternatively, by heating a planar nematic layer from below *heat focusing* [5] leads to anisotropic thermoconvection (ATC). The characteristic times in ATC are annoyingly long except when a large director-stabilizing planar magnetic field ($\|\hat{\mathbf{x}}$) is applied as in [8]. On the other hand, this system is interesting since its theoretical description is somewhat simpler than in EC.

In this paper we will concentrate on the “director-dominated regime” where the slow dynamics of the director field determines the longest characteristic-time scale. This regime corresponds to EC at low frequencies in the conduction regime and to ATC in the absence of (or at very small) stabilizing magnetic fields. Most of the experimental studies of EC have been performed until recently in this regime; the new weak-electrolyte effects [9,10] relevant for high frequencies, thin cells, or nematic materials with a very small dielectric anisotropy ϵ_a will not be included. In the director-dominated regime the sequences of spatio-temporal structures found experimentally by slowly increasing the main control parameter (the applied electric field in EC or the temperature gradient in ATC) are similar in both systems. Typically, normal rolls, with their axis $\perp \hat{\mathbf{x}}$, are found at onset [11,5]. They undergo, at rather small ϵ , the reduced distance to the convection threshold, modulational or homogeneous instabilities, leading toward either oblique rolls (zig-zags) [11–14] or abnormal rolls [15–17]. At higher ϵ bimodal or grid patterns [18,14] are very often found, which finally become oscillating [18–20]. Despite the fact that some elements of these scenarios (especially the last steps implying stationary or oscillating bimodal structures) have been known experimentally for more than 20 years in EC, a comprehensive theoretical description and explanation are still lacking.

Since all the bifurcations occur relatively near to the convection threshold, one major theoretical approach consists in the “order-parameter expansions.” Order parameters are introduced as the amplitudes of the *dynamically active modes*, e.g., the pattern-forming, critically slowed roll modes (of growth rate $\sigma \sim \epsilon$) in the framework of the standard weakly nonlinear (WNL) analysis. A simplified description of the dynamics of the system is then obtained in terms of “amplitude” or “order-parameter equations,” where the nonlinearities are truncated at cubic order in the common super-

*Present address: Laboratoire d’Énergétique et de Mécanique Théorique et Appliquée, 2 av. de la Forêt de Haye, 54504 Vandoeuvre Cedex, France.

critical case [21]. The general structure of these equations and the allowed couplings between the amplitudes can be deduced *a priori* from the symmetries of the system. Nevertheless, a trustworthy description requires a systematic calculation of the coefficients from the basic “microscopic” equations; indeed, except in very simple cases, even the sign of the coefficients is not intuitively known. In nematic convection the standard WNL analysis results in either “Landau” (without spatial variations) or “Ginzburg-Landau” (including spatial degrees of freedom) amplitude equations [3,6]. They have allowed successful studies of many generic phenomena near threshold [7,20,23,24]. Some secondary instabilities of the roll structures have been qualitatively explained as well [25,26]. However, strong quantitative discrepancies concerning the long-wavelength secondary instabilities could only be resolved by the use of fully numerical solutions of the basic equations in which all the nonlinearities are kept (“Galerkin computations” [27,28]). Such methods were also needed to identify the surprising bifurcation to abnormal rolls in EC [15]. Heavy computations of this kind cannot easily be extended to bimodal structures; thus their stability has not been addressed theoretically up to now. In any case, the physical origin of bifurcations is hard to extract by numerical methods, whereas a transparent investigation of *nonlinear mechanisms* becomes possible within the order-parameter approach [26,29].

The main goal of this paper is to demonstrate that an order-parameter approach which includes a *homogeneous twist rotation* of the director as a new active mode allows us, in most cases, to reconstruct the whole sequence of bifurcations. The corresponding new order parameter φ , which defines to lowest order the angle between the average in-plane director \mathbf{n}_0 and $\hat{\mathbf{x}}$ [see Eq. (39)], has been in fact successfully introduced at first for nematic convection with homeotropic (isotropic) alignment [30]. In the planar case, the introduction of this new active mode stems naturally from the results of the Galerkin computations and the experiments in EC [15] and from a careful study of the results of the WNL analysis in ATC [29]. After a brief glance at the basic equations and their symmetries in Sec. II and at the standard linear properties in Sec. III A, we show in Sec. III B that this twist mode has only a slightly negative growth rate as compared to the growth rate of the roll modes. In Sec. IV the coupled amplitude equations for the roll and twist modes are calculated from the basic nematohydrodynamic equations, and we show that the twist mode can indeed become active. A quantitative description of the bifurcation to abnormal rolls is achieved. In Sec. V the amplitude equations are generalized to include long-wavelength modulations together with the mean-flow effects. A coupling between splay-twist modulations of the in-plane director and the mean flow is shown to give a very efficient secondary mechanism for the zig-zag instability. A subsequent restabilization of abnormal rolls at higher ϵ is also obtained. The competition between the various instabilities is analyzed. Section VI is devoted to the study of the short-wavelength instabilities of abnormal or oblique rolls. The amplitude equations of Sec. IV are generalized by the introduction of a secondary roll amplitude. It is shown that the mechanism towards the bimodal varicose, proposed in [26] for ATC on the basis of a WNL analysis, applies generally. Further investigation of the coupled amplitude equa-

tions reveals the existence of a Hopf bifurcation, which explains the oscillating bimodals. The microscopic mechanisms controlling the various bifurcations and the structure of the new solutions are systematically analyzed. Comparisons with numerical results and experimental findings concerning mainly the nematic materials N5 in EC and 5CB in ATC (Sec. II A) are presented whenever possible. We also propose a heuristic interpretation of the bifurcation scenarios, in terms of a competition (or “frustration”) between the focusing mechanisms and the viscous torques exerted on the in-plane director (Sec. IV D). The appendixes contain additional information concerning the linear equations (Appendix A), the calculational method (Appendix B), analytic approximations of some nonlinear coupling coefficients (Appendix C), and results for the nematic material MBBA (Appendix D).

II. BASIC EQUATIONS — SYMMETRIES

In Sec. II A we recall the basis of the standard nematohydrodynamic [1,3] description of EC and ATC; a detailed presentation can be found in [25] for EC and in [23,29] for ATC. The dimensionless units and the sets of material parameters used are also introduced. Section II B is devoted to the symmetry properties of the system and to the basic expansion techniques.

A. Basic nematohydrodynamic equations — dimensionless units

The director dynamics is determined by

$$\gamma_1 \mathbf{n} \times \dot{\mathbf{n}} = \mathbf{n} \times \mathbf{h}, \quad (1)$$

where γ_1 is an anisotropic viscosity, and the dot stands for the material derivative $\partial_t + \mathbf{v} \cdot \nabla$. The molecular field \mathbf{h} [Eq. (3) of [25]] contains elastic contributions proportional to the splay, twist, and bend constants k_{11} , k_{22} , and k_{33} , an electric contribution proportional to the dielectric anisotropy ϵ_a in EC, and finally viscous contributions \mathbf{h}_v . A convenient form is

$$\mathbf{h}_v = -\alpha_2 \underline{\underline{D}} \cdot \mathbf{n} - \alpha_3 \mathbf{n} \cdot \underline{\underline{D}}, \quad (2)$$

where $\underline{\underline{D}}$ is the tensor gradient of velocity, $D_{ij} = \partial v_i / \partial x_j$. Since the anisotropic viscosity α_2 is negative and of much larger absolute value than the anisotropic viscosity α_3 , the main term $\propto \alpha_2$ in Eq. (2) tends to rotate \mathbf{n} in such a way that the director-transverse velocity gradients $\mathbf{n} \times (\underline{\underline{D}} \cdot \mathbf{n})$ are minimized [29].

The evolution equation for the velocity \mathbf{v} reads

$$\rho_m \dot{\mathbf{v}} = \mathbf{f}_{\text{vol}} - \nabla p + \underline{\underline{\text{div}}} \underline{\underline{\sigma}}, \quad (3)$$

with ρ_m the fluid density and p the pressure. The stress tensor $\underline{\underline{\sigma}}$ [Eq. (7) of [25]] contains elastic contributions and viscous contributions proportional to the anisotropic viscosities $\alpha_1, \dots, \alpha_6$. We will also use the Miesowicz viscosities $\nu_a = \alpha_4/2$, $\nu_b = \nu_a + (\alpha_3 + \alpha_6)/2$, and $\nu_c = \nu_a + (\alpha_5 - \alpha_2)/2$, and refer to the corresponding flow geometries a, b , and c [1].

Differences between EC and ATC come into play in the expression of the bulk force \mathbf{f}_{vol} in Eq. (3) or equivalently in

TABLE I. (a) Dimensionless units, from [7], used for electroconvection (EC). (b) Dimensionless units, from [23,29], used for anisotropic thermoconvection (ATC).

Quantity	Scaling unit	Interpretation of the scaling unit
(a)		
Elastic constant	$k_0 = 10^{-12}$ N	
Viscosity	$\alpha_0 = 10^{-3}$ kg m ⁻¹ s ⁻¹	
Dielectric constant	$\epsilon_0 = 8.854 \times 10^{-12}$ F m ⁻¹	permittivity of free space
Electric conductivity	$\sigma_0 = 10^{-8} (\Omega \text{ m})^{-1}$	
Mass density	$\alpha_0^2/k_0 = 10^6$ kg m ⁻³	
Length	d/π	inverse of typical roll wave number
Time	$\tau_{\text{DD}} = \alpha_0 d^2 / (k_0 \pi^2)$	typical vertical director- diffusion time
Electric potential	$V_0 = \pi \sqrt{k_0 / \epsilon_0}$	typical Fréedericksz threshold
(b)		
Elastic constant	k_{11}	splay elastic constant
Viscosity	$\nu_a = \alpha_4 / 2$	isotropic viscosity
Heat conductivity	κ_{\perp}	conductivity perpendicular to the director
Length	d/π	inverse of typical roll wave number
Time	$\tau_{\text{TD}} = d^2 / (\kappa_{\perp} \pi^2)$	vertical thermal-diffusion time
Temperature	$\nu_a \kappa_{\perp} \pi^3 / (\alpha g_0 d^3)$	

the nature of the scalar field which drives the convection instability. In EC, it is the modulation ϕ of the electric potential which determines the electric field

$$\mathbf{E} = \frac{\sqrt{2} V_{\text{app}}}{d} [\cos(\omega t) \hat{\mathbf{z}} - d \nabla \phi], \quad (4)$$

with V_{app} the effective applied voltage and d the thickness of the cell. The modulation of the electric potential is related to the ionic charge density ρ_e through the Maxwell equation $\rho_e = \nabla \cdot [\epsilon_{\perp} \mathbf{E} + \epsilon_a (\mathbf{n} \cdot \mathbf{E}) \mathbf{n}]$, and its evolution is governed by charge conservation,

$$\dot{\rho}_e = -\nabla \cdot [\sigma_{\perp} \mathbf{E} + \sigma_a (\mathbf{n} \cdot \mathbf{E}) \mathbf{n}], \quad (5)$$

where σ_{\perp} and σ_a are anisotropic conductivities. The bulk force is then [right hand side of Eq. (2.59) of [3]]

$$\mathbf{f}_{\text{vol}} = \rho_e \mathbf{E} + (\mathbf{P} \cdot \nabla) \mathbf{E}, \quad (6)$$

i.e., the sum of the Coulomb force and of the (purely non-linear) ponderomotive force which implies the macroscopic polarization \mathbf{P} . This latter term had never been systematically included in theoretical studies of EC, but it has turned out to have very little influence on the phenomena we study.

In ATC, the relevant scalar field is the difference $\theta = T - (T_0 - \Delta T_{\text{app}} z/d)$ between the actual temperature T and the conductive profile, with T_0 the mean temperature, and $\Delta T_{\text{app}}/d$ the thermal gradient applied between the lower and upper plates of the convection cell. The evolution of θ is governed by the heat-diffusion equation

$$\dot{\theta} = \nabla \cdot [\kappa_{\perp} \nabla T + \kappa_a (\mathbf{n} \cdot \nabla T) \mathbf{n}], \quad (7)$$

where κ_{\perp} and κ_a are anisotropic thermal diffusivities. Under the standard Boussinesq approximation the bulk force reads

$$\mathbf{f}_{\text{vol}} = -\rho_m [1 - \alpha(T - T_0)] g_0 \hat{\mathbf{z}}, \quad (8)$$

with α the thermal expansion coefficient, g_0 the gravitational acceleration.

We assume as usual the incompressibility condition $\nabla \cdot \mathbf{v} = 0$ and introduce the velocity potentials f and g such that

$$v_x = \partial_x \partial_z f + \partial_y g, \quad v_y = \partial_y \partial_z f - \partial_x g, \quad v_z = -(\partial_x^2 + \partial_y^2) f. \quad (9)$$

Since n_x can be eliminated from the equations by using the normalization condition $\mathbf{n}^2 = 1$, the local state vector of the fluid is finally

$$V = (\phi, n_y, n_z, f, g) \quad \text{in EC,}$$

$$V = (\theta, n_y, n_z, f, g) \quad \text{in ATC.} \quad (10)$$

The basic equations [Eqs. (5), (1), and (3) for EC, Eqs. (7), (1) and (3) for ATC] take the form

$$D \cdot \partial_t V = L_R \cdot V + N_2(V, V) + N_3(V, V, V) + \text{h.o.t.}, \quad (11)$$

where D and L_R are linear, N_2 and N_3 are nonlinear differential operators, and h.o.t. denotes ‘‘higher-order terms.’’ In the following, we will, for example, refer to the first line of Eq. (11) as the ϕ equation (in EC) and to the corresponding nonlinearities as $N_{2\phi}, N_{3\phi}$, etc. The main control parameter R , with the dimensionless units of Table I, is given by

$$R = \left(\frac{V_{\text{app}}}{V_0} \right)^2 \quad \text{in EC,} \quad R = \frac{\alpha g_0 d^3}{\nu_a \kappa_{\perp} \pi^4} \Delta T_{\text{app}} \quad \text{in ATC.} \quad (12)$$

The applied electric field reads $E_{\text{app}} = \sqrt{2R} \cos \omega t = \sqrt{2RE_{ac}}$ in EC. Note that for not too thin layers the largest characteristic time in EC is the director-diffusion time τ_{DD} [Table I(a)], followed by the charge-diffusion time $\tau_{\text{CD}} = \epsilon_{\perp} / \sigma_{\perp}$, and the viscous-diffusion time $\tau_{\text{VD}} = 2\rho_m d^2 / (\alpha_4 \pi^2)$. To allow a direct comparison with [15,25] we will display our results as a function of $\omega_{\text{CD}} = \tau_{\text{CD}} \omega$. Note that

TABLE II. (a) Dimensionless parameters for the nematics N5 and MBBA used in EC (see text; note that we have always assumed $\rho'_m = 10^{-3}$). (b) Dimensionless parameters for the nematic 5CB used in ATC (see text).

		(a)												
		k'_{11}	k'_{22}	k'_{33}	α'_1	α'_2	α'_3	α'_4	α'_5	α'_6	ϵ'_\parallel	ϵ'_\perp	σ'_\parallel	σ'_\perp
N5		9.8	4.6	11.4	-39.0	-109.3	1.5	56.3	82.9	-24.9	5.106	5.29	7.48	4.4
MBBA		6.66	4.2	8.61	-18.1	-110.4	-1.1	82.6	77.9	-33.6	4.72	5.25	1.5	1
		(b)												
		k'_{11}	k'_{22}	k'_{33}	α'_1	α'_2	α'_3	α'_4	α'_5	α'_6	κ'_a	F	Pr	
5CB		1	0.634	1.303	-0.184	-2.343	-0.132	2	1.90	-0.575	0.663	790	440	

$$\frac{\tau_{DD}}{\tau_{CD}} = Q \frac{\sigma'_\perp}{\epsilon'_\perp}, \quad \text{where} \quad Q = \frac{\alpha_0 d^2 \sigma_0}{k_0 \pi^2 \epsilon_0}, \quad (13)$$

and the primes denote the dimensionless material constants. In ATC the director-diffusion time $\tau_{DD} = \gamma_1 d^2 / (k_{11} \pi^2)$ also exceeds by far the thermal-diffusion time τ_{TD} [Table I(b)] and the viscous-diffusion time τ_{VD} , as measured by the (large) dimensionless numbers

$$F = \frac{\tau_{DD}}{\tau_{TD}} = \frac{\kappa_\perp \gamma_1}{k_{11}}, \quad Pr = \frac{\tau_{TD}}{\tau_{VD}} = \frac{\alpha_4}{2 \rho_m \kappa_\perp}. \quad (14)$$

Table II displays the material parameters used for the calculations. We have focused on standard nematic materials: N5 = Merck Phase 5 at 30 °C with the parameters defined in [15] for EC; 5CB at 27 °C with the parameters in [8] for ATC. In Appendix D, however, results will be given in EC for another common nematic material, MBBA at 25 °C, introduced as MBBA I in [7].

B. Symmetries — expansion techniques

We consider as usual the idealization of a nematic layer infinitely extended in the horizontal plane. The resulting translational invariance implies that the full solutions of Eq. (11) can be written as a superposition of horizontal Fourier modes characterized by their *horizontal wave vector* $\mathbf{q} = q \hat{\mathbf{x}} + p \hat{\mathbf{y}}$, e.g., in ATC,

$$V = \sum_{\mathbf{q}} (\theta^{\mathbf{q}}(z), n_y^{\mathbf{q}}(z), n_z^{\mathbf{q}}(z), f^{\mathbf{q}}(z), g^{\mathbf{q}}(z)) e^{i\mathbf{q} \cdot \mathbf{r}}, \quad (15)$$

where $\mathbf{r} = x \hat{\mathbf{x}} + y \hat{\mathbf{y}}$ is the horizontal position in the layer. The case of EC is very similar, except that θ is replaced by ϕ , and that the fields become time dependent. For a discussion of the symmetry properties of the EC equations with respect to transformations of time, see [27]; as usual only the lowest nontrivial Fourier components in time are kept in this paper. With respect to the vertical dependence (in z), all fields have to vanish at the boundaries $z = \pm \pi/2$ in our scaling. Using a standard Galerkin technique [31], θ (or ϕ), n_y , n_z , and g are expanded in a sine basis $\{S_n(z) = \sin[n(z + \pi/2)]\}$. For the vertical velocity potential f , which must fulfill $f = \partial_z f = 0$ at the boundaries, the Chandrasekhar basis $\{C_n(z)\}$ [32] is

used. We keep at least the two leading vertical modes for each field in order to obtain a good numerical accuracy of typically 2% as compared with calculations with many modes. On the other hand, by keeping only one vertical mode for each field *analytic* semiquantitative results (with an accuracy of typically 10%) can be obtained [33]. Therefore our results will often be exemplified under this ‘‘one-mode approximation’’ which captures the essential physical features.

Another global symmetry of the system is the reflection symmetry $S: y \mapsto -y$. The corresponding symmetry of Eq. (11) is

$$S: y \mapsto -y, \quad n_y \mapsto -n_y, \quad g \mapsto -g,$$

$$\text{with the other fields unchanged,} \quad (16)$$

or equivalently for a Fourier mode in Eq. (15),

$$(\theta^{\mathbf{q}}, n_y^{\mathbf{q}}, n_z^{\mathbf{q}}, f^{\mathbf{q}}, g^{\mathbf{q}}) e^{i\mathbf{q} \cdot \mathbf{r}} \mapsto (\theta^{\mathbf{q}}, -n_y^{\mathbf{q}}, n_z^{\mathbf{q}}, f^{\mathbf{q}}, -g^{\mathbf{q}}) e^{i\mathbf{q} \cdot S(\mathbf{r})},$$

where it should be noted that $\mathbf{q} \cdot S(\mathbf{r}) = S(\mathbf{q}) \cdot \mathbf{r}$. Consequently, the solutions V of Eq. (11) can be classified according to their symmetry: if $S(V) = V$, the symmetry S is not broken; otherwise V and $S(V)$ are two degenerate variants of the same global state.

The reflection with respect to the midplane of the layer, $z \mapsto -z$, is also a global symmetry. Two types of Fourier modes in Eq. (15) can be distinguished according to their transformation under this reflection: type + when $\theta^{\mathbf{q}}(z)$ [or $\phi^{\mathbf{q}}(z)$], $n_z^{\mathbf{q}}(z)$, $f^{\mathbf{q}}(z)$ are even, $n_y^{\mathbf{q}}(z)$, $g^{\mathbf{q}}(z)$ are odd; type – in the opposite case. Introducing $\text{sym}(a) = \pm 1$ according to the type of the Fourier mode $a = (\theta, n_y, n_z, f, g) e^{i\mathbf{q} \cdot \mathbf{r}}$, Eq. (11) have the important ‘‘Boussinesq-like’’ symmetry property

$$\text{sym}[N_2(a, b)] = -\text{sym}(a)\text{sym}(b),$$

$$\text{sym}[N_3(a, b, c)] = +\text{sym}(a)\text{sym}(b)\text{sym}(c). \quad (17)$$

III. ACTIVE MODE BASIS FOR THE EXTENDED WNL ANALYSIS

WNL analyses in general rely on a perturbative treatment of the nonlinear terms in the evolution Eq. (11) for small amplitudes of convection. Thus they become asymptotically exact in the limit $\epsilon \rightarrow 0$, but in practice, as well as in our case, semiquantitative or qualitative results are often obtained even when the amplitudes are not infinitesimal [21]. Within this perturbative approach it is natural to focus at first on the *linearized evolution equations* $D\partial_t V = L_R V$, and to calculate the corresponding eigenmodes as the solutions of $\sigma DV = L_R V$. The solutions of the full problem (11) are then constructed as superpositions of these linear eigenmodes. Among those, the *dynamically active modes* are the modes of positive growth rate σ , and in addition the modes of slightly negative growth rate σ which are nonlinearly excited by coupling with the modes of $\sigma > 0$ [36]. The associated expansion coefficients are the ‘‘amplitudes’’ or ‘‘order parameters.’’ Their evolution equations will be calculated after adiabatic elimination of the remaining expansion coefficients associ-

ated with the *dynamically passive modes* of negative growth rate; see [21] or Appendix B. For planar nematic convection, the standard family of active modes consists of the roll modes, the properties of which are reviewed in Sec. III A. However, in Sec. III B it is shown that diffusion modes of the director have also to be considered as active, even quite close to the convection threshold.

A. Standard active mode basis: the roll modes

The first studies of EC [4,7] and ATC [5] have shown that the modes destabilizing the quiescent solution $V=0$ of Eq. (11) are *roll modes* of wave number $|\mathbf{q}|$ close to 1 (i.e., of half period $\approx d$ in physical units) and of the z symmetry type $+$. These roll modes are the solutions of

$$\sigma(\mathbf{q};R)DV_1(\mathbf{q};R) = L_R V_1(\mathbf{q};R), \quad (18)$$

where the eigenvalues $\sigma(\mathbf{q};R)$ are always real in the absence of weak-electrolyte effects [9] and correspond to the growth rates. In the one-mode approximation the eigenvectors read

$$V_1(\mathbf{q};R) = \begin{cases} ((\tilde{\phi}e^{-i\omega t} + \tilde{\phi}^*e^{i\omega t})S_1(z), \tilde{n}_y S_2(z), i\tilde{n}_z S_1(z), \tilde{f}C_1(z), \tilde{g}S_2(z))e^{i\mathbf{q}\cdot\mathbf{r}} & \text{in EC,} \\ (\tilde{\theta}S_1(z), \tilde{n}_y S_2(z), i\tilde{n}_z S_1(z), \tilde{f}C_1(z), \tilde{g}S_2(z))e^{i\mathbf{q}\cdot\mathbf{r}} & \text{in ATC,} \end{cases} \quad (19)$$

Since V in Eq. (11) is real, $V_1(-\mathbf{q};R) = (V_1(\mathbf{q};R))^*$ holds, and one can focus on the modes with $\mathbf{q} \cdot \hat{\mathbf{x}} \geq 0$. Then, a phase choice can be made such that $\tilde{n}_z = 1$, $\text{Re}(\tilde{\phi})$, $\text{Im}(\tilde{\phi})$, $\tilde{\theta}$ and \tilde{f} are positive (real) numbers, and \tilde{n}_y and \tilde{g} are real numbers. The focusing mechanisms are the following ones (see also the linear equations in Appendix A). In EC, a splay-bend director fluctuation (field n_z) excites a charge or potential modulation (field ϕ) via the charge-focusing term $-\sigma_a Q E_{ac} \partial_x n_z$ in the ϕ equation (A1); a mass flow (field f) is induced via the Coulomb force (A6); this flow reinforces the initial director distortion via the viscous torque $+|\alpha_z| \partial_x v_z$ in the n_z equation (A3). In ATC, a splay-bend distortion of the director leads to a temperature modulation (field θ) via the heat-focusing term $-\kappa_a R \partial_x n_z$ in the heat equation (A1); a flow is excited by the buoyancy force (A7); this flow reinforces the initial director distortion exactly as in EC.

When the destabilizing forces overcome the stabilizing ones, i.e., when R exceeds R_c , the growth rate $\sigma(\mathbf{q};R)$ of the so-called critical roll mode at $\mathbf{q} = \mathbf{q}_c$ becomes positive. By continuity, when $R > R_c$, there exists a wave-vector band of roll modes of positive growth rates, which can be, for $\epsilon = R/R_c - 1$ not too large, written as

$$\sigma(\mathbf{q};R) \approx \frac{R - R_0(\mathbf{q})}{\tau_q R_c} = \frac{\epsilon - \epsilon_0(\mathbf{q})}{\tau_q}. \quad (20)$$

$R_0(\mathbf{q})[\epsilon_0(\mathbf{q})]$ is the (reduced) threshold of the roll mode \mathbf{q} (‘‘neutral surface’’), and τ_q is a characteristic time. Note that $\epsilon_0(\mathbf{q}_c) = 0$, and that τ_{q_c} is the characteristic time τ of the

instability [34]. The symmetry properties discussed in Sec. II lead to the distinction between two types of roll modes [35]: the *normal rolls*, of wave vector \mathbf{q} parallel to $\hat{\mathbf{x}}$, where \mathcal{S} (16) is not broken, consequently $n_y = g = 0$: normal rolls are purely two-dimensional modes; and the *oblique rolls*, of wave vector $\mathbf{q} = q\hat{\mathbf{x}} + p\hat{\mathbf{y}}$ with $qp \neq 0$, where \mathcal{S} is broken. Consequently two variants exist: the ‘‘zigs’’ with $q, p > 0$ and the ‘‘zags’’ with $q > 0, p < 0$. These modes are three dimensional since n_y and g are nonzero (nevertheless the vertical averages of n_y and g vanish).

In ATC one has critical normal rolls [23]. In EC, at low ω one finds critical oblique rolls, whereas for ω larger than the *Lifshitz* frequency $\omega_L = 0.8\tau_{CD}^{-1}$ the critical modes are of the normal-roll type. At large ω , but still below the crossover frequency to the dielectric regime ($\omega_D = 4.0\tau_{CD}^{-1}$), the charge-focusing mechanism becomes less efficient. Consequently, the convection only sets in with narrower rolls (q_c increases with ω), where all gradients increase for compensation, and at higher voltages (R_c increases with ω). In this ‘‘high-energy’’ limit where also the dielectric torque stabilizing the planar configuration gets very large, the damping constant $1/\tau$ of the ‘‘forced’’ roll mode is very large.

B. The director modes

At fixed \mathbf{q} , in addition to the roll modes $V_1(\mathbf{q};R)$ (19), there exists an infinite number of linear eigenmodes $V_m(\mathbf{q};R)$ with discrete eigenvalues $\sigma_m(\mathbf{q};R)$. For R close to R_c , the corresponding growth rates $\text{Re}(\sigma_m(\mathbf{q};R))$ are nega-

tive for all m and \mathbf{q} and typically maximal in the *homogeneous* case $\mathbf{q}=\mathbf{0}$ [37]. In our regime where the damping of the director field is by far the weakest, the small values of $|\text{Re}(\sigma_m(\mathbf{0};R))|$ are associated with director modes. They are determined by the linear diffusion equations for n_y and n_z with $\partial_x=\partial_y=0$ (then \mathbf{n} does not couple with the other fields):

$$\gamma_1 \partial_t n_y = k_{22} \partial_z^2 n_y, \quad \gamma_1 \partial_t n_z = (k_{11} \partial_z^2 + \epsilon_a R) n_z \quad (21)$$

for EC [see, e.g., Eq. (A3)]. The equations for ATC are similar except for the absence of the dielectric torque ($\propto \epsilon_a$). The system (21) admits two families of linear eigenmodes: the n_y

modes $n_y=S_m(z), n_z=0$, and the n_z modes $n_y=0, n_z=S_m(z)$. We call the modes of largest growth rate [for $m=1$, i.e., with an even cosine profile $S_1(z)=\cos(z)$] the twist mode and the splay mode, respectively. For the twist mode

$$V_T=(0, S_1(z), 0, 0, 0), \quad (22)$$

with the notations (10), one finds, e.g., the growth rate

$$\sigma_T = -\frac{k_{22}}{\gamma_1} \text{ in EC}, \quad \sigma_T = -\frac{k_{22}}{F} \text{ in ATC}. \quad (23)$$

The ratio of σ_T to the growth rate of the critical roll mode is

$$\frac{\sigma_T}{\sigma(\mathbf{q}_c; \epsilon)} = \tau \sigma_T \epsilon^{-1} \simeq \begin{cases} -\frac{k_{22}}{k_{33}q_c^2 + k_{22}p_c^2 + k_{11} - \epsilon_a R_c} \epsilon^{-1} & \text{in EC} \\ -\frac{k_{22}}{k_{33}q_c^2 + k_{22}p_c^2 + k_{11}} \epsilon^{-1} & \text{in ATC}, \end{cases} \quad (24)$$

where simple approximations of the characteristic times τ have been used [see Fig. 1(a) for a comparison with rigorous calculations in EC]. The order of magnitude of the ratio (24) is $-k_{22}/(k_{33}+k_{11})\epsilon^{-1} \simeq -0.25\epsilon^{-1}$: it is very negative only for very small ϵ . The twist mode should therefore be included in the active mode basis. Indeed, we will show in Sec. IV that its slow linear damping can be compensated either at quadratic order [term $N_2(V, V)$ in Eq. (11)] or at cubic order [term $N_3(V, V, V)$ in Eq. (11)] by a coupling with two roll modes. On the other hand, the splay mode $V_S=(0, 0, S_1(z), 0, 0)$, which has a growth rate of the same magnitude as σ_T , can only be excited at cubic order for symmetry reasons [38]. We have checked that the excitation of V_S always occurs far above the threshold ϵ_{AR} of excitation of V_T (Sec. IV). Therefore the splay mode will not be kept in the active mode basis here. Note that the *quasihomogeneous* twist modes with long-wavelength variations of small wave vector \mathbf{q} play no role for perfect roll or bimodal structures and have only to be considered in the case of modulated structures (Sec. V).

IV. NONLINEAR ROLL SOLUTIONS

The inclusion of the twist mode in the active mode basis lifts the simple symmetry rules which exclude quadratic

resonant terms in the standard amplitude equations. Thus the treatment of the quadratic nonlinearities requires some care; for this reason a general extended WNL scheme is introduced in Appendix B. In Sec. IV A this scheme is applied to calculate the amplitude equations which couple the amplitude A of a roll mode to the amplitude φ of the twist mode [Eq. (29)]. In Sec. IV B the abnormal-roll solutions of these equations are studied, and in Sec. IV C the oblique-roll solutions are studied. The nonlinearities controlling the values of all the coefficients introduced in Sec. IV A are given. This allows one to give a precise physical interpretation of the mechanisms involved and to introduce in Sec. IV D a general principle to interpret the roll-twist interactions.

A. Calculation of the roll-twist amplitude equations

We apply the scheme of Appendix B to roll structures of fixed wave vector \mathbf{q} . Only two active modes have to be considered: the roll mode $V_1(\mathbf{q})$ (19) and the twist mode V_T (22). According to Eqs. (B8) and (B12), the corresponding WNL solution assumes the form

$$V = V_A + V_\perp = [A V_1(\mathbf{q}) + \text{c.c.}] + \varphi V_T + V_\perp, \quad (25)$$

where the passive part reads

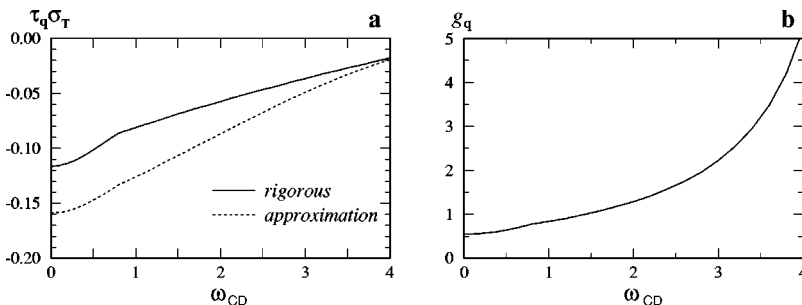


FIG. 1. In EC (for N5), as a function of the dimensionless frequency $\omega_{CD}=\tau_{CD}\omega$: (a) solid line: growth rate σ_T of the homogeneous twist mode, in units of the normal-roll characteristic time τ_q at $\mathbf{q}=\mathbf{q}_c\hat{\mathbf{x}}$. Dotted line: analytic approximation (24). (b) Saturation coefficient g_q (30) of the normal rolls.

$$\begin{aligned}
V_{\perp} = & -L^{-1}[N_2(V_A, V_A) - \langle U_1(\mathbf{q}), N_2(V_A, V_A) \rangle D V_1(\mathbf{q}) \\
& - \langle U_1(-\mathbf{q}), N_2(V_A, V_A) \rangle D V_1(-\mathbf{q}) \\
& - \langle U_T, N_2(V_A, V_A) \rangle D V_T].
\end{aligned}$$

$U_1(\mathbf{q})$ and U_T are the adjoint roll and twist modes [see Eq. (B3)]. Introducing the coefficients

$$\begin{aligned}
\beta_2(\mathbf{q}) &= \langle U_1(\mathbf{q}), N_2(V_1(\mathbf{q})|V_T) \rangle, \\
\gamma(\mathbf{q}) &= -\langle U_T, N_2(V_1(\mathbf{q})|V_1(-\mathbf{q})) \rangle,
\end{aligned} \quad (26)$$

one obtains

$$\begin{aligned}
V_{\perp} = & |A|^2 V_2(\mathbf{q}, -\mathbf{q}) + [A^2 V_2(\mathbf{q}, \mathbf{q}) + \text{c.c.}] \\
& + \varphi [A V_2(\mathbf{q}, T) + \text{c.c.}],
\end{aligned} \quad (27)$$

where

$$\begin{aligned}
V_2(\mathbf{q}, -\mathbf{q}) &= -L^{-1}[N_2(V_1(\mathbf{q})|V_1(-\mathbf{q})) + \gamma(\mathbf{q})D \cdot V_T], \\
V_2(\mathbf{q}, \mathbf{q}) &= -L^{-1}N_2(V_1(\mathbf{q}), V_1(\mathbf{q})), \\
V_2(\mathbf{q}, T) &= -L^{-1}[N_2(V_1(\mathbf{q})|V_T) - \beta_2(\mathbf{q})D \cdot V_1(\mathbf{q})].
\end{aligned} \quad (28)$$

By projecting Eq. (11) onto $U_1(\mathbf{q})$ and U_T [see also Eq. (B13)], one arrives at our first set of coupled amplitude equations

$$\partial_t A = \left(\frac{\epsilon - \epsilon_0(\mathbf{q})}{\tau_{\mathbf{q}}} - g_{\mathbf{q}}|A|^2 + \beta_2(\mathbf{q})\varphi - \beta_3(\mathbf{q})\varphi^2 \right) A, \quad (29a)$$

$$\partial_t \varphi = [\sigma_T - g_{\varphi}\varphi^2 + \Gamma(\mathbf{q})|A|^2]\varphi - \gamma(\mathbf{q})|A|^2, \quad (29b)$$

where additional coefficients have been defined:

$$\begin{aligned}
g_{\mathbf{q}} = & -\langle U_1(\mathbf{q}), N_2(V_1(\mathbf{q})|V_2(\mathbf{q}, -\mathbf{q})) \\
& + N_2(V_1(-\mathbf{q})|V_2(\mathbf{q}, \mathbf{q})) + N_3(V_1(\mathbf{q})|V_1(\mathbf{q})|V_1(-\mathbf{q})) \rangle,
\end{aligned} \quad (30)$$

$$\beta_3(\mathbf{q}) = -\langle U_1(\mathbf{q}), N_2(V_T|V_2(\mathbf{q}, T)) + N_3(V_T|V_T|V_1(\mathbf{q})) \rangle, \quad (31)$$

$$g_{\varphi} = -\langle U_T, N_3(V_T|V_T|V_T) \rangle = \frac{|\sigma_T|}{8}, \quad (32)$$

$$\Gamma(\mathbf{q}) = \Gamma_2(\mathbf{q}) + \Gamma_3(\mathbf{q}), \quad \text{with}$$

$$\begin{aligned}
\Gamma_2(\mathbf{q}) &= \langle U_T, N_2(V_1(\mathbf{q})|V_2(-\mathbf{q}, T)) \\
& + N_2(V_1(-\mathbf{q})|V_2(\mathbf{q}, T)) \rangle, \\
\Gamma_3(\mathbf{q}) &= \langle U_T, N_3(V_1(\mathbf{q})|V_1(-\mathbf{q})|V_T) \rangle.
\end{aligned} \quad (33)$$

Note that for $\varphi=0$, Eq. (29a) reduces to the well-known Landau equation for the roll amplitude A , describing a supercritical bifurcation since $g_{\mathbf{q}} > 0$. We have not scaled out $\tau_{\mathbf{q}}$ and $g_{\mathbf{q}}$ as usual, in order to clearly separate the linear and nonlinear effects controlling the value of A .

B. Rolls with a normal wave vector

The amplitude equations (29) must be invariant under the global symmetry \mathcal{S} (16), which transforms \mathbf{q} into $S(\mathbf{q})$ and φ into $-\varphi$. Therefore the coefficients $\beta_2(\mathbf{q})$ and $\gamma(\mathbf{q})$ vanish for rolls with a normal wave vector $\mathbf{q} = q\hat{\mathbf{x}}$ such that $\mathbf{q} = S(\mathbf{q})$. After elimination of $|A|^2$ in Eq. (29a) and insertion into (29b), one has to solve

$$[\sigma_T - g_{\varphi}\varphi^2 + \Gamma(\mathbf{q})|A(\mathbf{q}; \epsilon; \varphi)|^2]\varphi = 0 \quad (34)$$

for the stationary solutions. Clearly the branch $\varphi=0$ corresponds to the standard normal-roll solutions,

$$|A| = \sqrt{\frac{\epsilon - \epsilon_0(\mathbf{q})}{\tau_{\mathbf{q}}g_{\mathbf{q}}}}, \quad \varphi = 0. \quad (35)$$

The effect of the coefficient $\Gamma(\mathbf{q})$ in Eq. (29b), which turns out to be always positive, is to enhance a fluctuation of φ about the normal-roll solution (35). Indeed, two roots of the cubic equation in φ (34), which were complex at small ϵ , become real when ϵ gets larger than

$$\epsilon_{\text{AR}}(\mathbf{q}) = \epsilon_0(\mathbf{q}) + \epsilon'_{\text{AR}}(\mathbf{q}), \quad \text{where} \quad \epsilon'_{\text{AR}}(\mathbf{q}) = |\tau_{\mathbf{q}}\sigma_T| \frac{g_{\mathbf{q}}}{\Gamma(\mathbf{q})}. \quad (36)$$

At this point a bifurcation from normal ($\mathbf{q} \parallel \hat{\mathbf{x}}, \varphi=0$) to *abnormal rolls* ($\mathbf{q} \parallel \hat{\mathbf{x}}, \varphi \neq 0$) occurs, which corresponds to breaking the symmetry \mathcal{S} (16) without tilting the rolls (see [15] for an identification of this instability in EC). We will now study the coefficients determining the threshold of this bifurcation and the ensuing saturation of the twist amplitude φ ; if not otherwise stated, we will consider rolls at $q = q_c$.

1. Threshold of the abnormal-roll bifurcation

The abnormal-roll threshold $\epsilon_{\text{AR}}(\mathbf{q})$ (36) is controlled linearly by the growth rate σ_T of the twist mode in $\tau_{\mathbf{q}}^{-1}$ units, nonlinearly by the saturation factor $g_{\mathbf{q}}$ in the A equation (29a), and by the coupling coefficient $\Gamma(\mathbf{q})$ in the φ equation (29b).

In EC, the linear effects tend to favor the abnormal rolls at high ω , where $|\tau\sigma_T|$ becomes very small [Fig. 1(a)]. This indicates that the rotation of the director in the horizontal plane becomes relatively easier at high ω , as compared with the excitation of the splay-bend n_z mode associated with the roll modes [cf. Eq. (24) for $\tau\sigma_T = \epsilon\sigma_T/\sigma(\mathbf{q}; \epsilon)$, and the discussion in Sec. III A].

The first important nonlinear effect is the saturation of the amplitude expressed by the coefficient $g_{\mathbf{q}}$. This has been first studied systematically for ATC [29]. In EC, the most important saturating (positive) contributions are (P1) the contributions of $N_{3\phi}(V_1(\mathbf{q})|V_1(\mathbf{q})|V_1(-\mathbf{q}))$ due to $\frac{1}{2}\sigma_a Q E_{ac} \partial_x n_z^3$, which indicate that the charge focusing becomes less efficient with increasing n_z [compare with the linear term $-\sigma_a Q E_{ac} \partial_x n_z$ of Eq. (A1), quoted in Sec. III A, and note the opposite sign]; and (P2) the contributions of $N_{3n_z}(V_1(\mathbf{q})|V_1(\mathbf{q})|V_1(-\mathbf{q}))$ due to $\alpha_2(\partial_x v_z)n_z^2$, which indicate that the shear exerted on the director by the vertical flows diminishes when the director rotates upwards [compare with the linear term $-\alpha_2 \partial_x v_z$ in Eq. (A3)]. Both (P1) and

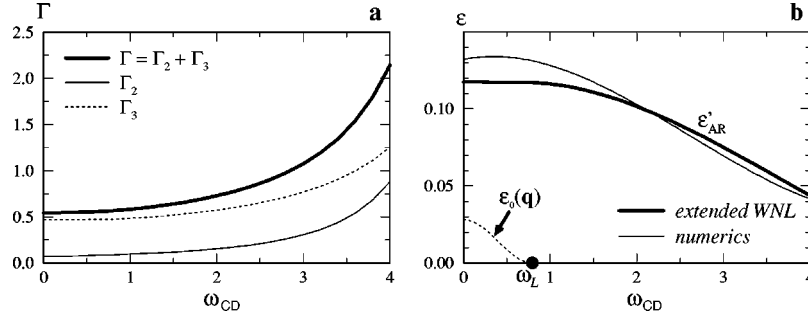


FIG. 2. In EC, for rolls with wave vector $\mathbf{q} = q_c(\omega)\hat{x}$: (a) nonlinear interaction coefficient $\Gamma(\mathbf{q})$ (thick line) between the roll and twist modes [cf. Eqs. (29b), (33)]. The contributions $\Gamma_2(\mathbf{q})$ (thin line) and $\Gamma_3(\mathbf{q})$ (dotted line) of the quadratic and cubic nonlinearities in the n_y equation are shown. (b) Reduced abnormal-roll threshold $\epsilon'_{AR}(\mathbf{q})$ obtained from the extended WNL expression (36) (thick line) or from the numerical computations [15] (thin line). The normal-roll threshold $\epsilon_0(\mathbf{q})$, only slightly positive for frequencies smaller than the Lifshitz frequency $\omega_L = 0.8\tau_{CD}^{-1}$, is shown with the dotted curve.

(P2) are generated by the quadratic corrections to n_x due to the distortion of the director field above onset of convection, i.e., by inserting in the equations $n_x = 1 - \frac{1}{2}(n_y^2 + n_z^2)$ from the director-normalization condition $\mathbf{n}^2 = 1$. We therefore call (P1) and (P2) “geometrical corrections” to the quoted linear terms, where $n_x = 1$ is taken. The dependence on $q_c(\omega)$ (corresponding to horizontal gradients) of the contributions (P1), together with the fact that $|\tilde{\phi}/\tilde{n}_z|$ in the linear mode (19) decreases strongly with ω , lead to a strong increase of the contributions (P1) to $g_{\mathbf{q}}$ when ω increases. The dependence on $q_c(\omega)$ of the contributions (P2) renders them also much larger when ω increases. The most important antisaturating (negative) contributions are (N1) the contributions of $N_{3n_z}(V_1(\mathbf{q})|V_1(\mathbf{q})|V_1(-\mathbf{q}))$ due to $\alpha_2(\partial_z v_x)n_z^2$, which indicate that when the director tilts upwards, it becomes sensitive to the horizontal flows which tilt the director further as do the vertical flows at linear order; (N2) the contributions of $N_{3n_z}(V_1(\mathbf{q})|V_1(\mathbf{q})|V_1(-\mathbf{q}))$ due to $-\frac{1}{2}\epsilon_a(E_{app})^2n_z^3$, which signify that the stabilizing dielectric torque [see Eq. (A4)] is reduced with increasing n_z ; and (N3) the contributions of $N_{3f}(V_1(\mathbf{q})|V_1(\mathbf{q})|V_1(-\mathbf{q}))$ due to the source term $(\alpha_1 + \alpha_2 + \alpha_3)\partial_x[(\partial_x v_z)n_z^2]$ in the evolution equation for v_z . This indicates a decrease of the effective viscosity for the vertical flows in the rolls, since with increasing n_z the highest Miesowicz viscosity geometry c is gradually left for these flows. The negative contributions (N1), (N2), (N3) increase less strongly with ω than the saturating ones (P1), (P2). Consequently $g_{\mathbf{q}}$ increases with ω [Fig. 1(b)]. Note that all the effects controlling the value of $g_{\mathbf{q}}$ in EC exist also in ATC [29], provided that the charge focusing in (P1) is replaced by the heat focusing (see Sec. 4.2 of [29]) or that the electric field in (N2) is replaced by a planar magnetic field (this was predicted to lead to a subcritical bifurcation in ATC in [23]).

The nonlinear coefficient directly responsible for the bifurcation (36) towards abnormal rolls is $\Gamma(\mathbf{q}) = \Gamma_2(\mathbf{q}) + \Gamma_3(\mathbf{q})$ (33). In Appendix C we give an analytic approximation of $\Gamma(\mathbf{q})$ within the one-mode approximation. The contribution $\Gamma_3(\mathbf{q})$ of the cubic nonlinearities indicates a renormalization of the damping of the twist mode by a coupling to the roll modes. It is dominated by the contributions of $\alpha_2(\partial_x v_x)n_z n_y$ in $N_{3n_y}(V_1(\mathbf{q})|V_1(-\mathbf{q})|V_T)$. The corresponding mechanism can be interpreted according to the principle that the director tends to rotate away from the

velocity gradients and therefore out of the (x, z) plane due to the α_2 term in Eq. (2). There exists also a secondary mechanism of elastic origin, due to the term $2(k_{33} - k_{22})(\partial_x n_z)^2 n_y$, which corresponds to a release of bend by twist. Since the bend energy is proportional to $q_c^2(\omega)$, this mechanism is only efficient in EC for the narrow rolls (of large q_c) at high frequency ω (Appendix C). The contribution $\Gamma_2(\mathbf{q})$ (33) of the quadratic nonlinearities indicates an indirect renormalization of the damping of φ , which occurs through the (possible) excitation of the quadratic mode $V_2(\mathbf{q}, T)$. In EC, $\Gamma_2(\mathbf{q})$ becomes large only at high ω [Fig. 2(a)]; in ATC, $\Gamma_2(\mathbf{q})$ is always one order of magnitude smaller than $\Gamma_3(\mathbf{q})$. The corresponding mechanisms are studied in Appendix C.

In EC, the increase of $\Gamma(\mathbf{q})$ with ω [Fig. 2(a)], favorable to the abnormal rolls [see Eq. (36)], is roughly compensated by the increase of $g_{\mathbf{q}}$ with ω [Fig. 1(b)]. Thus the decrease of the linear growth rate $|\tau\sigma_T|$ [Fig. 1(a)] appears to be the main cause for the decrease of the abnormal-roll threshold $\epsilon'_{AR}(\mathbf{q})$ (36) with increasing ω [Fig. 2(b)]. The values of $\epsilon'_{AR}(\mathbf{q})$ (36) match those of the fully nonlinear calculations [15] at high frequency. At low frequency, discrepancies show up which are due to nonlinear effects of higher order not included in Eq. (29). Their influence grows in the limit $\omega \rightarrow 0$, since there the bifurcation to abnormal rolls occurs at increasingly higher ϵ and A . In ATC, we find $\epsilon_{AR}(\mathbf{q}) = 0.11$, a value larger than ϵ_{ZZ} (Sec. V). This agrees with the experiments, where the normal rolls at small ϵ are first destabilized by zig-zag modulations [14].

2. Saturation of the abnormal-roll bifurcation

The saturation of the director rotation ($\varphi \neq 0$) in abnormal rolls appears to be *indirect*: it is not controlled by the classical saturating term $-g_{\varphi}\varphi^3$ in the φ equation (29b), but rather by the coupling term $-\beta_3(\mathbf{q})\varphi^2 A$ in the A equation (29a). Indeed, the abnormal-roll solutions of Eq. (29) read, for $\epsilon > \epsilon_{AR}(\mathbf{q})$,

$$|A| = a_{\mathbf{q}} \sqrt{\frac{1}{1+b_{\mathbf{q}}} \epsilon_{AR}(\mathbf{q}) + \frac{b_{\mathbf{q}}}{1+b_{\mathbf{q}}} \epsilon - \epsilon_0(\mathbf{q})},$$

$$\varphi = \pm \sqrt{\frac{1}{1+b_{\mathbf{q}}} \frac{\epsilon - \epsilon_{AR}(\mathbf{q})}{\tau_{\mathbf{q}} \beta_3(\mathbf{q})}}, \quad (37)$$

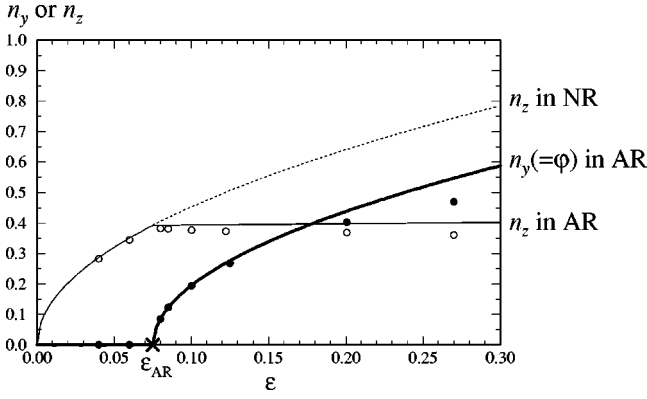


FIG. 3. Director amplitudes $n_z(\epsilon)$ (thin line) and $n_y(\epsilon) = \varphi(\epsilon)$ (solid line) for EC in roll solutions at $\mathbf{q} = q_c \hat{\mathbf{x}}, \omega_{CD} = 3$ [see Eq. (38)]. The normal roll (NR) branch $n_z(\epsilon) \sim \sqrt{\epsilon}, \varphi(\epsilon) = 0$ becomes unstable at $\epsilon = \epsilon_{AR}$ with respect to the twist mode. In the subsequent abnormal rolls (AR), $n_z(\epsilon)$ remains roughly constant, whereas $\varphi(\epsilon)$ increases as $\sqrt{\epsilon - \epsilon_{AR}}$ [see Eq. (37)]. The open and closed circles show the numerical results [15] for $n_z(\epsilon)$ and $\varphi(\epsilon)$, respectively.

with $a_q = 1/\sqrt{\tau_q g_q}, b_q = g_q g_\phi / [\beta_3(\mathbf{q}) \Gamma(\mathbf{q})]$. This latter coefficient is always small, for instance, in EC $b_q = 0.077$ at $\omega_{CD} = 0.5$ and $b_q = 0.0015$ at $\omega_{CD} = 4$, while in ATC, $b_q = 0.034$. Thus, to lowest order in b_q , the amplitude A stays constant for $\epsilon > \epsilon_{AR}$, and the saturation of φ is clearly due to the β_3 effect. For q near $q_c, \beta_3(\mathbf{q})$ is always positive, indicating a negative feedback $\varphi \rightarrow A$ in Eq. (29b). In EC and ATC, two leading contributions of $N_3(V_T, V_T, V_1(\mathbf{q}))$ dominate all the other ones in $\beta_3(\mathbf{q})$. One leading contribution is due to $\frac{1}{2} \sigma_a Q E_{app} \partial_x (n_y^2 n_z)$ from $N_{3\phi}(V_T, V_T, V_1(\mathbf{q}))$ in EC and $\frac{1}{2} \kappa_a R \partial_x (n_y^2 n_z)$ from $N_{3\theta}(V_T, V_T, V_1(\mathbf{q}))$ in ATC. These terms are geometrical corrections [analogous in principle to the term (P1) of Sec. IV B 1] to the focusing-mechanism terms in Eqs. (A1) and (A2) for the scalar field. These terms indicate that a director rotation away from the roll wave vector (n_y large) diminishes the charge and heat focusing. The second dominant contribution to $\beta_3(\mathbf{q})$ (31) is, both in EC and ATC, due to the term $-|\alpha_2| n_y^2 (\partial_x v_z)$ from $N_{3n_z}(V_T, V_T, V_1(\mathbf{q}))$. It is a correction to the linear torque $|\alpha_2| \partial_x v_z$ in the n_z equation (A3), which indicates that when the director rotates, the shear inducing of the n_z modulation also becomes less efficient. In EC, $\beta_3(\mathbf{q})$ drastically increases with the frequency: $\beta_3 = 0.036$ at $\omega \approx 0$, while $\beta_3 = 2.99$ at $\omega_{CD} = 4$. This is mainly due to the fact that the roll modes at high frequency become more sensitive to the ϕ and n_z effects mentioned above. Typical amplitudes $n_z(\epsilon)$ and $\varphi(\epsilon)$ of the n_z and n_y distortions given in abnormal-roll solutions by

$$\begin{aligned} n_z &= -n_z(\epsilon) S_1(z) \sin \mathbf{q} \cdot \mathbf{r} + \text{h.o.t.} \\ &= -2A(\epsilon) S_1(z) \sin \mathbf{q} \cdot \mathbf{r} + \text{h.o.t.}, \\ n_y &= \varphi(\epsilon) S_1(z) + \text{h.o.t.}, \end{aligned} \quad (38)$$

according to Eqs. (25), (19), and (22), are shown for EC at an intermediate frequency in Fig. 3. Note that φ determines to lowest order the in-plane director at the midplane of the layer since there [39]

$$\begin{aligned} \mathbf{n} &= \hat{\mathbf{x}} \sqrt{1 - n_y^2 - n_z^2} + \hat{\mathbf{y}} n_y + \hat{\mathbf{z}} n_z = \mathbf{n}_0 + \hat{\mathbf{z}} n_z + \text{h.o.t.}, \\ &\text{with } \mathbf{n}_0 = \hat{\mathbf{x}} + \hat{\mathbf{y}} \varphi. \end{aligned} \quad (39)$$

Note also that the order-parameter scheme up to cubic order breaks down if n_z or φ becomes larger than 1. The amplitudes $n_z(\epsilon) = 2A(\epsilon)$ and $\varphi(\epsilon)$ (37) match the numerical predictions of [15] only for ϵ not too large, such as $\epsilon \leq 0.2$ in the example of Fig. 3. At higher ϵ , the values of $\varphi(\epsilon)$ (37) get systematically much larger than those given by the fully nonlinear Galerkin computations. Indeed, the saturation of φ in Eq. (29) is very weak; i.e., in the full equations, higher-order effects not included in the order-parameter approach come into play at these high ϵ , high φ values. The deviations become more important at low ω in EC, where β_3 is very small and thus $\varphi(\epsilon)$ (37) reaches 1 for rather small ϵ , e.g., for $\epsilon \approx 0.15$ at $\omega \approx 0$.

There exist special cases where $\beta_3(\mathbf{q})$ can become negative, i.e., the abnormal-roll bifurcation does not saturate in the framework of Eqs. (29) [40]. This occurs in EC at low frequency for q larger than q_c , e.g., $q > 1.20q_c$ at $\omega_{CD} = 1$, or in ATC for $q > 1.45q_c$. The important negative term in $\beta_3(\mathbf{q})$, which counteracts the effect of the positive terms discussed here above, is a contribution of $N_{3n_z}(V_T, V_T, V_1(\mathbf{q}))$ due to $\frac{1}{2} (2k_{22} - 3k_{33}) n_y^2 \partial_x^2 n_z$. It signifies a reinforcement of elastic origin of the n_z distortion in rolls when the director rotates towards $\pm \hat{\mathbf{y}}$. Such ‘‘narrow abnormal rolls’’ are nevertheless obtained in the Galerkin computations, where apparently higher-order terms not included in Eq. (29) become important.

C. Oblique rolls

In the case of zigs of wave vector $\mathbf{q} = q \hat{\mathbf{x}} + p \hat{\mathbf{y}}$ with $q, p > 0$, the coefficients $\gamma(\mathbf{q})$ and $\beta_2(\mathbf{q})$ in Eq. (29) are nonzero. The symmetry rule (16) now only imposes that $\gamma(\mathbf{q})$ and $\beta_2(\mathbf{q})$ change sign when passing from the zig \mathbf{q} to the zag $S(\mathbf{q}) = q \hat{\mathbf{x}} - p \hat{\mathbf{y}}$. The corresponding stationary solutions of Eq. (29) can still be calculated by elimination of A and solution of a cubic equation in φ , but the expressions become quite lengthy. The result is the existence of a ‘‘generalized abnormal-roll threshold’’ $\epsilon_{AR}(\mathbf{q})$, which reduces to Eq. (36) for $p=0$, and which increases with increasing $|p|$. For $\epsilon < \epsilon_{AR}(\mathbf{q})$ only one root is real, i.e., only one solution branch exists; whereas for $\epsilon > \epsilon_{AR}(\mathbf{q})$ all the three roots are real, i.e., two additional solution branches appear. Since the new solutions, which one might call ‘‘anomalous’’ oblique rolls [41], are typically unstable against long-wavelength perturbations (except under certain conditions at rather large ϵ , see, e.g., [15]), we will discuss here only the structure of the first, most stable solutions. They are well approximated at small ϵ by the standard WNL solutions, where the cubic effects in φ are neglected, i.e., $\beta_3, g_\phi, \Gamma = 0$ in Eq. (29). One finds, with $c_q = \beta_2(\mathbf{q}) \gamma(\mathbf{q}) / (g_q |\sigma_T|)$,

$$|A| = a_q \sqrt{\frac{\epsilon - \epsilon_0(\mathbf{q})}{1 + c_q}}, \quad \varphi = -\frac{\gamma(\mathbf{q})}{|\sigma_T|} |A|^2. \quad (40)$$

In zigs ($p > 0$), due to the ‘‘torque’’ $-\gamma(\mathbf{q}) |A|^2$ in the φ Eq. (29b), where $\gamma(\mathbf{q})$ is always positive, the director rotates

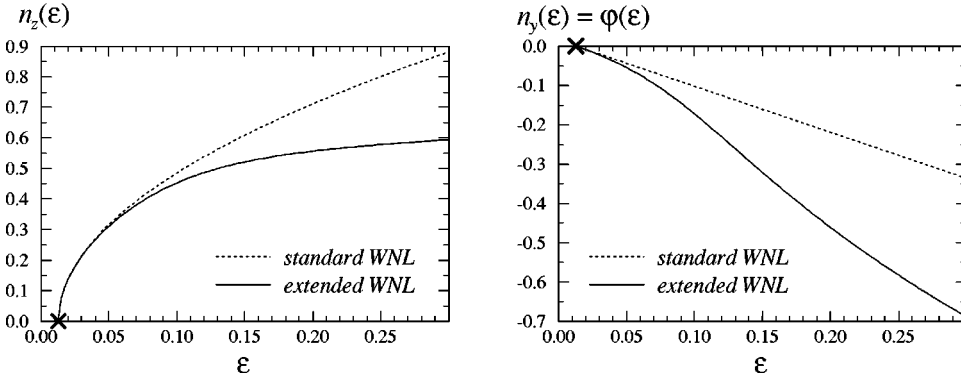


FIG. 4. In ATC (for 5CB), comparison between results of the standard WNL theory and the extended WNL theory [i.e., $\Gamma, \beta_3 \neq 0$ in Eq. (29)] for the amplitude of n_z (left) and of the twist mode (right) in an oblique-roll solution of Eq. (29). The linear threshold $\epsilon_0(\mathbf{q}) = 0.013$ is marked with the crosses. Note the increasing deviations from the WNL results $A \propto \sqrt{\epsilon - \epsilon_0(\mathbf{q})}, \varphi \propto [\epsilon - \epsilon_0(\mathbf{q})]$.

($\varphi < 0$) towards the direction of the axis of the rolls or, equivalently, away from the wave vector ($p\varphi < 0$). This effect has been in fact pointed out in [26,29] for ATC. The quadratic nonlinearities of the n_y equation which control the value of $\gamma(\mathbf{q})$ (26) are the advection term $-\gamma_1 v_z \partial_z n_y$, the α_2 terms $\alpha_2(\partial_x v_x^f) n_y$ and $|\alpha_2|(\partial_z v_y^f) n_z$ [the superscript f denoting the velocity components generated by the potential f , see Eq. (9)], and the elastic term (only important in EC) $-(k_{11} + k_{33} - 2k_{22})(\partial_x n_z)(\partial_y n_z)$. Since the α_2 contributions are in general dominant, this torque exerted by the rolls on the director can also be understood from the principle that the director tends to avoid the velocity gradients. The saturation of the roll amplitude in Eq. (40) is clearly enhanced by the β_2 effect [cf. $c_q \propto \beta_2(\mathbf{q})$]. Indeed, since $\beta_2(\mathbf{q})$ is positive for all zigs at $q \approx q_c$ in the normal-roll regime (usual case in ATC, case $\omega > \omega_L$ in EC), the $+\beta_2(\mathbf{q})\varphi A$ term in Eq. (29a) indicates that the rotation of the director towards $-\hat{\mathbf{y}}$ in zigs ($\varphi < 0$) induces a negative feedback on A (as does also the β_3 term, but at a higher order). We find that $\beta_2(\mathbf{q})$ (26) is dominated by two contributions of $N_2(V_T, V_1(\mathbf{q}))$. The first one comes from the term $-\sigma_a Q E_{\text{app}} \partial_y(n_y, n_z)$ in the electric potential equation in EC and from the term $-\kappa_a R \partial_y(n_y, n_z)$ in the heat equation in ATC. The second dominant contribution arises both in EC and ATC from the term $|\alpha_2| n_y(\partial_y v_z)$ in the n_z equation. These terms are corrections to the linear focusing term [see Eqs. (A1) and (A2)] and to the viscous torque in the n_z equation (A3). They also signify that a director rotation away from the direction of the wave vector ($p n_y < 0$) reduces the efficiency of the focusing mechanisms of convection (A diminishes).

The simple expressions Eq. (40) of the standard WNL oblique-roll solutions are of course modified by the inclusion of the effects of β_3, g_φ , and Γ in Eq. (29). The corrections read at small ϵ

$$\delta|A| = -a_q^3 \frac{\gamma(\mathbf{q})[\beta_2(\mathbf{q})\Gamma(\mathbf{q}) + \beta_3(\mathbf{q})\gamma(\mathbf{q})]}{2(1+c_q)^{5/2}|\sigma_T|^2 g_q} [\epsilon - \epsilon_0(\mathbf{q})]^{3/2},$$

$$\delta\varphi = \frac{\gamma(\mathbf{q})}{|\sigma_T|^2} \frac{\beta_3(\mathbf{q})\gamma^2(\mathbf{q})/g_q |\sigma_T| - \Gamma(\mathbf{q})}{1+c_q} |A|^4. \quad (41)$$

Because of the Γ and β_3 effects, $\delta|A| < 0$: the roll amplitude is always strongly reduced due to the in-plane director rotation, as shown in Fig. 4 for ATC. The full solutions of Eq. (29) have been calculated for a representative experimental oblique-roll wave vector $\mathbf{q} = 1.07q_c(\hat{\mathbf{x}} \cos 8^\circ + \hat{\mathbf{y}} \sin 8^\circ)$ [14].

The amplitudes plotted in Fig. 4 are still defined according to Eq. (38); in fact in oblique rolls there is also a periodic contribution of the roll mode (19) to n_y , but this contribution $\propto A(\epsilon)\tilde{n}_y$ is dominated by the contribution $\propto \varphi(\epsilon)$ even at very small ϵ values, e.g., for $\epsilon \geq 0.04$ in the example of Fig. 4. The strong deviation from the standard WNL law $n_z(\epsilon), A(\epsilon) \propto \sqrt{\epsilon - \epsilon_0(\mathbf{q})}$ (40), has been observed experimentally [20] (see Fig. 9a there), and constitutes an experimental confirmation of our analysis for ATC. The correction to the WNL solution (40) for $\varphi, \delta\varphi$ (41), is usually negative (as in Fig. 4) since $g_q |\sigma_T| \Gamma(\mathbf{q}) > \beta_3(\mathbf{q}) \gamma^2(\mathbf{q})$. Provided the reduction of A due to the β_3 term is not too strong, the angle $|\varphi|$ increases because of the Γ effect. It is only when β_3 gets very large, for instance, for the oblique rolls at \mathbf{q}_c in EC at very low frequency, that the φ corrections can become positive: the reduction of A is then so strong that the angle of the in-plane rotation is diminished. Note that the range of ϵ where the standard WNL solutions (40) remain a good approximation typically extends with increasing p . The continuous transformation from a quasilinear law $\varphi(\epsilon) \propto -[\epsilon - \epsilon_0(\mathbf{q})]$ at large p [cf. Eq. (40)] to the square root law $\varphi(\epsilon) \propto -\sqrt{\epsilon - \epsilon_{\text{AR}}}$ at $p=0$ [cf. Eq. (37)] is visible in Fig. 2 of [15]. Thus the zig solutions $p > 0, \varphi < 0$ are continuously attached to the abnormal-roll solutions with $\varphi < 0$ in Eq. (37). It appears therefore justified to introduce as a generalized definition of ‘‘zigs’’ the criterion $\varphi < 0$, with which both the oblique rolls with $p > 0, \varphi < 0$ and the abnormal rolls with $p = 0, \varphi < 0$ are considered to belong to the same class of solutions.

In some special cases $\beta_2(\mathbf{q})$ can become negative in zigs for $p > 0$, i.e., the in-plane director rotation reinforces the roll amplitude to lowest order [c_q becomes negative in Eq. (40)]. This occurs first in the oblique-roll regime in EC for $\omega < \omega_L$. Then, at $q = q_c$, $\beta_2(\mathbf{q})$ is slightly negative for $0 < p \leq p_c$ and becomes positive for $p \geq p_c$. The important negative term in $\beta_2(\mathbf{q})$, which counteracts the positive terms discussed above, is a contribution of $N_{2n_z}(V_1(\mathbf{q}), V_T)$ due to $2(k_{33} - k_{22})\partial_x(\partial_y n_z)n_y$. It implies an elastic reinforcement of the n_z distortion in zigs when the director rotates towards $-\hat{\mathbf{y}}$. This term leads also, at fixed p , to a decrease of $\beta_2(\mathbf{q})$ with increasing q . Thus in EC and ATC in the normal-roll range, $\beta_2(\mathbf{q})$ can become negative at fixed p for q larger than q_c (e.g., at $p = 0.05q_c$, for $q > 1.19q_c$ in ATC, for $q > 1.04q_c$ in EC at $\omega_{\text{CD}} = 1$).

D. Interpretation: director–wave-vector frustration

The amplitude equations (29) display, in the most common normal-roll regime (when $\mathbf{q}_c = q_c \hat{\mathbf{x}}$, and $\mathbf{q} = q \hat{\mathbf{x}} + p \hat{\mathbf{y}}$ is

not too far from \mathbf{q}_c), the competition between two opposite tendencies. On the one hand, the roll dynamics Eq. (29a) is controlled in this regime by the fact that $\beta_2(\mathbf{q})p > 0$, $\beta_3(\mathbf{q}) > 0$, these coefficients being dominated by nonlinear corrections to the linear focusing mechanism terms (in the loose sense, i.e., including all the terms contributing to the instability loop quoted in Sec. III A, in particular, the viscous torque in the n_z equation). These β_2 and β_3 terms change the linear growth rate of the roll modes (20) into an effective (“nonlinear”) growth rate

$$\sigma^{\text{eff}}(\mathbf{q}; \epsilon) = \frac{\epsilon - \epsilon_0(\mathbf{q})}{\tau_{\mathbf{q}}} + \beta_2(\mathbf{q})\varphi - \beta_3(\mathbf{q})\varphi^2.$$

This effective growth rate is maximal for $\varphi = \varphi_{\text{opt}}(\mathbf{q}) = \beta_2(\mathbf{q})/[2\beta_3(\mathbf{q})]$. Since $\varphi_{\text{opt}}(\mathbf{q})$ is typically between 0 and p/q , this means that (M1) the focusing mechanisms are more efficient when the roll wave vector is roughly parallel to the director. On the other hand, the dynamics of the twist mode Eq. (29b) is controlled in this regime by the fact that $\gamma(\mathbf{q})p > 0, \Gamma(\mathbf{q}) > 0$. These coefficients are dominated by the α_2 contributions signifying the tendency of the director to rotate due to the viscous torques away from the velocity gradients and therefore away from the wave vector of the rolls. The γ and Γ terms thus indicate that (M2) the director is pushed by the rolls away from their wave vector. The competition between (M1) and (M2) results in a “director-wave vector frustration.” A first manifestation of this frustration is the bifurcation from the normal to the abnormal rolls, in which the rolls almost “destroy” themselves: in abnormal rolls the director rotation is clearly due to (M2), and the subsequent saturation of the roll amplitude ($|A| \sim \text{const}$ for $\epsilon > \epsilon_{\text{AR}}$) due to (M1). We will see in the rest of the paper that this frustration has other important consequences.

V. LONG-WAVELENGTH ZIG-ZAG INSTABILITY OF ROLLS WITH A NORMAL WAVE VECTOR

In EC for frequencies larger than the Lifshitz frequency ω_L , or in ATC for usual nematics, one finds near onset normal rolls at $\mathbf{q} = \mathbf{q}_c = q_c \hat{\mathbf{x}}$. According to Sec. IV, these normal rolls can undergo a secondary bifurcation to abnormal rolls at rather small $\epsilon = \epsilon_{\text{AR}}$. However, another possible secondary bifurcation is the long-wavelength zig-zag instability, where undulations along the roll axis are amplified. This instability is a generic feature of planar nematic convection [27], which thus competes with the abnormal-roll instability (cf. Fig. 3 of [15]). On the basis of a WNL analysis in EC, a first mechanism has been identified for the zig-zag instability, which relies on the coupling with the so-called mean-flow modes [25]. These are passive modes that are excited by roll undulations, but since their adiabatic elimination can lead to nonanalyticities, a separate equation [analogous in principle to Eq. (B11)] has to be kept for them. Nevertheless, strong discrepancies have remained between the results of the standard WNL analysis as exposed in [25,23] and the Galerkin computations or the experiments. Typically, the standard WNL thresholds for the long-wavelength instabilities are much too large as was noted in [27] for EC and in [14] for ATC. In this section we want to show that these

discrepancies can be resolved by taking into account additional cubic nonlinearities [Eq. (46)], which couple the twist mode and two roll modes. These terms are considered to be of higher order in the standard WNL approach. We will also analyze in detail the microscopic mechanisms controlling the zig-zag instability and the subsequent restabilization of the abnormal rolls in EC.

A. Roll-twist-mean-flow amplitude equations

To describe long-wavelength instabilities, the scheme introduced in Sec. IV A has to be generalized in order to calculate modulated-roll solutions. The scheme must also be combined with the method explained in [25] to extract the (possibly) singular mean flow. One starts with a superposition of roll modes (19)

$$V_{\text{rolls}} = \int_{\mathcal{V}(\mathbf{q}_c)} d\mathbf{q} A(\mathbf{q}) V_1(\mathbf{q}) + \text{c.c.} \approx A(\mathbf{r}) V_1(\mathbf{q}_c) + \text{c.c.}, \quad (42)$$

where $\mathcal{V}(\mathbf{q}_c)$ is a domain centered around \mathbf{q}_c , and the slowly varying envelope

$$A(\mathbf{r}) = \int_{\mathcal{V}(\mathbf{q}_c)} d\mathbf{q} A(\mathbf{q}) e^{i(\mathbf{q} - \mathbf{q}_c) \cdot \mathbf{r}} \quad (43)$$

has been introduced.

The long-wavelength part V_{LW} of the solution is then defined to lowest order by

$$\begin{aligned} D\partial_t V_{\text{LW}} - LV_{\text{LW}} &= I_2 \\ &= \int_{\mathcal{V}(\mathbf{0})} ds \int_{\mathcal{V}(\mathbf{q}_c)} d\mathbf{q} A(\mathbf{q}) \\ &\quad \times A(-\mathbf{q} + \mathbf{s}) N_2(V_1(\mathbf{q}) | V_1(-\mathbf{q} + \mathbf{s})). \end{aligned} \quad (44)$$

The velocity field in Eq. (44) can be treated with the technique introduced in [25]. One solves for a modified right hand side where only the source term in the g field is retained and projected onto the Hagen-Poiseuille profile $P_1(z) = \frac{1}{2}(\pi^2/4 - z^2)$ according to $I_{2g} \rightarrow \langle I_{2g} \rangle = (6/\pi^2) \langle P_1(z), I_{2g}(s; z) \rangle$; this gives the mean-flow contribution. We also isolate the twist amplitude φ as the amplitude of $S_1(z)$ in the n_y field of V_{LW} [cf. Eq. (22)] and get after adiabatic elimination of the other fields

$$\begin{aligned} V_{\text{LW}} &= \int_{\mathcal{V}(\mathbf{0})} ds [\varphi(\mathbf{s}) V_T e^{i\mathbf{s} \cdot \mathbf{r}} + G(\mathbf{s}) V_{\text{MF}} e^{i\mathbf{s} \cdot \mathbf{r}} + V_{\text{LW}}^{\text{rest}}(\mathbf{s})] \\ &= \varphi(\mathbf{r}) V_T + G(\mathbf{r}) V_{\text{MF}} + \int_{\mathcal{V}(\mathbf{0})} ds V_{\text{LW}}^{\text{rest}}(\mathbf{s}), \end{aligned} \quad (45)$$

with $V_{\text{MF}} = (0, 0, 0, P_1(z))$.

Finally, there are passive, short-wavelength contributions to the solution. The harmonics about $\pm 2\mathbf{q}_c$ are standard. Additionally, we take into account the terms generated by $N_2(V_1(\mathbf{q}) | V_T e^{i\mathbf{s} \cdot \mathbf{r}})$, with wave vectors around $\pm \mathbf{q}_c$. The resulting quadratic modes $V_{2T}(\mathbf{q}, \mathbf{s})$ are calculated with the projector technique of Appendix B. They contribute to the

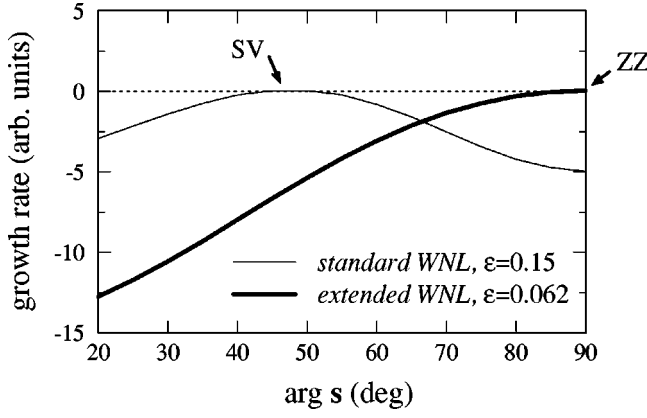


FIG. 5. Growth rates of long-wavelength perturbation modes $\delta V = a_+ V_1(\mathbf{q}_c + \mathbf{s}) + a_- V_1(\mathbf{q}_c - \mathbf{s})$ of the normal rolls at $\mathbf{q} = \mathbf{q}_c$ in ATC as a function of the modulation angle $\arg(\mathbf{s})$. The prediction of a zig-zag instability at $\epsilon = \epsilon_{ZZ} = 0.062$ from the extended WNL analysis (thick line) agrees with full numerical results and the experiments. The standard WNL analysis (thin line) predicts erroneously a skewed-varicose instability at $\arg(\mathbf{s}) \approx 50^\circ$, $\epsilon = \epsilon_{SV} = 0.15$.

solution with an amplitude $A\varphi$. The *higher-order terms* that we include in our analysis are the terms of order $A^2\varphi$ generated by these quadratic modes and directly by the coupling of the twist mode with the roll modes: we add to the right hand side I_2 of Eq. (44) a contribution

$$I_3 = \int_{\mathcal{V}(\mathbf{0})} ds \int_{\mathcal{V}(\mathbf{q}_c)} d\mathbf{q} \int_{\mathcal{V}(-\mathbf{q}_c)} d\mathbf{q}' \varphi(\mathbf{s}) A(\mathbf{q}) A(\mathbf{q}') \\ \times [(N_2(V_{2T}(\mathbf{q}, \mathbf{s}) | V_1(\mathbf{q}')) + N_2(V_{2T}(\mathbf{q}', \mathbf{s}) | V_1(\mathbf{q})) \\ + N_3(V_1(\mathbf{q}) | V_1(\mathbf{q}') | V_T e^{i\mathbf{s} \cdot \mathbf{r}})]. \quad (46)$$

This addition is consistent with the scheme of Sec. IV A, since a particular contribution of Eq. (46) in the n_y equation leads for $(\mathbf{s}, \mathbf{q}, \mathbf{q}') = (\mathbf{0}, \mathbf{q}_c, -\mathbf{q}_c)$ to the term $+\Gamma(\mathbf{q}_c) |A|^2 \varphi$ responsible of the abnormal-roll bifurcation. The important point is that Eq. (46) also induces corrections to the mean-flow equations which turn out to resolve the difficulties quoted in our Introduction. For instance, in ATC the standard WNL analysis predicts a skewed-varicose instability of the critical normal rolls at $\epsilon_{SV} = 0.15$, in contradiction to the experimental findings which show rather a zig-zag instability at much smaller ϵ ($\epsilon_{ZZ} \approx 0.05$ according to Fig. 4 of [14]). The inclusion of the terms (46) in the perturbation analysis of normal rolls drastically changes the form of the growth rate as a function of the modulation angle (Fig. 5) and leads to a zig-zag instability at $\epsilon_{ZZ} = 0.062$ comparable to the experiments. Since the zig-zag modulations are also for EC the most dangerous destabilizing modes of rolls with a normal wave vector, we now disregard the general skewed-varicose case. Using the method exposed, for instance, in [25], we apply an inverse Fourier transform to the evolution equations

for $A(\mathbf{q})$, $\varphi(\mathbf{s})$, and $G(\mathbf{s})$ obtained in Fourier space. This yields from expansions of the coefficients in powers of the wave vectors corresponding derivative terms. One arrives at the following system of equations for the roll envelope A , the twist amplitude φ , and the mean-flow amplitude G :

$$\tau \partial_t A = [\epsilon(1 - e_3 \partial_y^2) + r_2 \partial_y^2] A - |A|^2 A - a_7 |A|^2 \partial_y^2 A \\ - a_8 A^2 \partial_y^2 A^* - a_9 (\partial_y A)^2 A^* - a_{10} |\partial_y A|^2 A - i s_1 A \partial_y G \\ - i b_1 A \partial_y \varphi - i b_2 \varphi \partial_y A - \beta \varphi^2 A, \quad (47a)$$

$$\partial_t \varphi = (\sigma_T + K_1 \partial_y^2) \varphi + i \gamma' (A^* \partial_y A - A \partial_y A^*) \\ - g_\varphi \varphi^3 + \Gamma_\varphi |A|^2 \varphi, \quad (47b)$$

$$0 = \nu_b \partial_y^2 G + i q_4 \partial_y^2 (A^* \partial_y A - A \partial_y A^*) + \Gamma_G \partial_y^2 (|A|^2 \varphi), \quad (47c)$$

where we have recalled on the left hand side some of the time-derivative terms [42]. Note that the A equation has been multiplied by the characteristic time τ , and that the roll modes have been rescaled for convenience by a factor $a_{\mathbf{q}_c} = 1/\sqrt{\tau g_{\mathbf{q}_c}}$ (this amounts to rescaling the amplitudes by a factor $1/a_{\mathbf{q}_c}$). Some coefficients in Eq. (47) are linked to the coefficients appearing in Eq. (29) for nonmodulated rolls:

$$b_2 = \tau \left. \frac{\partial \beta_2(\mathbf{q}_c + p \hat{\mathbf{y}})}{\partial p} \right|_{p=0}, \quad \beta = \tau \beta_3(\mathbf{q}_c), \\ \gamma' = a_{\mathbf{q}_c}^2 \frac{1}{2} \left. \frac{\partial \gamma(\mathbf{q}_c + p \hat{\mathbf{y}})}{\partial p} \right|_{p=0}, \quad \Gamma_\varphi = a_{\mathbf{q}_c}^2 \Gamma(\mathbf{q}_c). \quad (48)$$

A typical set of coefficients is given for EC in Table III. Note that to lowest order in the amplitudes (47) reduces to the anisotropic Ginzburg-Landau equation for A if φ and G are adiabatically eliminated or to the roll-mean-flow system (35), (36) of [25] if φ is adiabatically eliminated. In Secs. V B and V C we will study the stability of the normal-roll solutions $A = \sqrt{\epsilon}$, $\varphi = 0$ of Eqs. (47), and in Sec. V D we will study the stability of the abnormal-roll solutions $A = \sqrt{(\epsilon_{AR} + b\epsilon)/(1+b)}$, $\varphi = \sqrt{(\epsilon - \epsilon_{AR})/[\beta(1+b)]}$ of Eqs. (47), where $\epsilon_{AR} = -\sigma_T/\Gamma_\varphi$ and $b = g_\varphi/(\beta\Gamma_\varphi)$.

B. Stability of normal rolls: Standard zig-zag mechanisms

The results of the standard WNL analysis concerning the zig-zag instability of normal rolls are recovered if the cubic terms implying the twist amplitude φ are dropped in Eq. (47), i.e., if one assumes $\Gamma_\varphi = \Gamma_G = 0$ (β and g_φ do not intervene at this stage). In contrast to [25] the twist amplitude φ has not been adiabatically eliminated. Thus the contribution of the twist dynamics appears now explicitly [43] in our formula for the zig-zag threshold,

TABLE III. Coefficients of the roll-twist-mean-flow amplitude equations (47), in EC for N5 at $\omega_{CD} = 1.5$.

e_3	r_2	a_7	a_8	a_9	a_{10}	s_1	b_1	b_2	β	σ_T	K_1	γ'	g_φ	Γ_φ	ν_b	q_4	Γ_G
0.17	0.10	-0.20	0.027	0.28	0.33	2.0	0.19	0.23	0.26	-0.042	0.088	0.16	0.0052	0.37	16.4	4.54	36.8

TABLE IV. Coefficients determining the standard zig-zag threshold (49) for the critical normal rolls in ATC (first line), and in EC at two different frequencies (second and third line). Note that the largest contributions to d_2 (49) are always the twist contribution $2b_1\gamma'/\sigma_T$ and the mean-flow contribution $2s_1q_4/\nu_b$.

	r_2	e_3	$a_7 - a_8$	$2b_1\gamma'/\sigma_T$	$2s_1q_4/\nu_b$	d_2
ATC	0.22	0.29	-1.05	-3.29	1.16	-1.13
EC at $\omega_{CD}=1$	0.033	0.26	-0.22	-0.83	1.22	+0.43
EC at $\omega_{CD}=2$	0.158	0.085	-0.25	-2.09	1.07	-1.19

$$\epsilon_{ZZ}^s = \frac{r_2}{d_2}, \quad \text{with} \quad d_2 = e_3 + a_7 - a_8 + \frac{2b_1\gamma'}{\sigma_T} + \frac{2s_1q_4}{\nu_b}. \quad (49)$$

The numerator r_2 is the square of the coherence length in the y direction, which vanishes at the Lifshitz point in EC: $r_2 \rightarrow 0^+$ when $\omega \rightarrow \omega_L^+$; the denominator d_2 has to be positive for a destabilization to occur. Since b_1 and γ' are always positive (and $\sigma_T < 0$), the *twist contribution* $2b_1\gamma'/\sigma_T$ is negative, i.e., stabilizing. The coefficients b_1 and γ' appear to be dominated by the same nonlinearities as β_2 and γ (Sec. IV C): the fact that the rolls get stiffer by an excitation of the twist is also a direct consequence of the ‘‘frustration’’ (Sec. IV D). This becomes clear by inspection of the n_z and n_y fields generated by a zig-zag perturbation of the normal rolls. Using the fact that the amplitudes for the modulation wave vectors $\pm p\hat{y}$ in a long-wavelength instability are almost opposite, one finds to lowest order in the perturbation amplitude a :

$$\frac{n_z}{\bar{n}_z} \simeq [-2A \sin(q_c x) + a \cos(q_c x) \sin(py)] S_1(z) \\ \simeq -2A \sin\left[q_c x - \frac{a}{2A} \sin(py)\right] S_1(z), \quad (50a)$$

$$\varphi \simeq aA \frac{\gamma'}{|\sigma_T|} p \cos(py). \quad (50b)$$

The zig-zag perturbation creates locally some obliqueness of the rolls, i.e., a modulated q_y component of the local wave vector, $q_y = -(a/2A)p \cos(py)$. According to (M2) (Sec. IV D), the in-plane director in the regions of obliqueness is pushed away from the local wave vector: this creates the splay-twist modulation (50b) (Fig. 7) [44]. According to (M1), the feed-back of this twist modulation on the roll perturbation is negative. The only destabilizing terms in d_2 (49) are the one of e_3 (at least at not too large frequency ω in EC) and more importantly the *mean-flow contribution* $2s_1q_4/\nu_b$, where s_1 and q_4 are always positive [45]. The zig-zag perturbation (50a) creates the mean flow

$$v_x = (\partial_y G) P_1(z) \simeq aA \frac{q_4}{\nu_b} p^2 \sin(py) P_1(z) \quad (51)$$

sketched in Fig. 7. In EC and ATC, important contributions to q_4 are given by the viscous terms in the v_x equation $\alpha_5[\partial_y(D_{xx}n_y) + \partial_z(D_{xx}n_z)]$, where $D_{xx} = \partial_x v_x^f = \partial_x^2 \partial_z f$. They signify anisotropic viscous mechanisms of creation of the

mean flow, quite different from the standard advection mechanisms (due to the term $\mathbf{v} \cdot \nabla v_x$ in the v_x equation) relevant for isotropic fluids where $q_4 < 0$. In EC, additionally the term $2\epsilon_{\perp} R(\partial_x \phi)(\partial_y^2 \phi)$ from the x component of the Coulomb force gives large contributions to q_4 . It corresponds to an electric mechanism of generation of the mean flow. The coefficient s_1 in Eq. (47a) is dominated by the contributions of $-\gamma_1 v_x \partial_x n_z$ in the n_z equation for EC and for ATC. Thus the mean flow (51), by advection of the director field in the rolls, reinforces the zig-zag perturbation (Fig. 7). In ATC, this primary zig-zag mechanism cannot compensate the stabilizing twist contribution, as shown in the first line of Table IV: $d_2 < 0$ in Eq. (49), i.e., no zig-zag instability is predicted by the standard WNL analysis. The twist contribution is overcompensated by the mean-flow one only at low frequencies in EC, for instance at $\omega_{CD}=1$ (second line of Table IV). At higher ω , b_1 and $-2b_1\gamma'/\sigma_T$ increase strongly, and d_2 also becomes negative (see, e.g., the third line of Table IV). The increase of the twist contributions results from the contribution to b_1 due to term $\epsilon_a R \partial_y(n_y n_z)$ in the z component of the Coulomb force. This term introduces an electric mechanism of stabilization of the zig-zag perturbation by the twist (note that it would become destabilizing for nematics with $\epsilon_a > 0$) which is only impor-

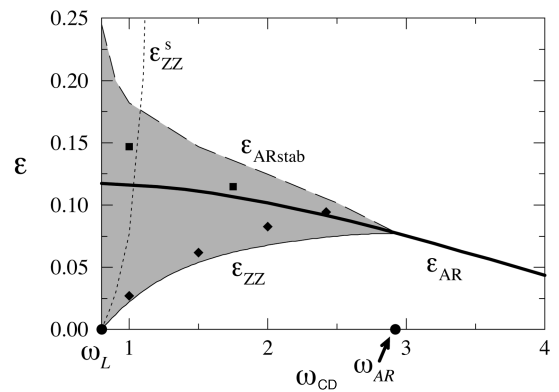


FIG. 6. Stability diagram for rolls at $\mathbf{q} = q_c \hat{x}$ in EC calculated from Eqs. (47), as a function of the dimensionless frequency $\omega_{CD} = \tau_{CD}\omega$. The unstable regions are in gray. For $\omega_L < \omega < \omega_{AR}$, the normal rolls are first destabilized at ϵ_{ZZ} (52a) towards oblique rolls by a zig-zag instability. For $\omega > \omega_{AR}$, the first instability is at ϵ_{AR} towards stable abnormal rolls. Abnormal rolls exist in general above ϵ_{AR} and restabilize for $\omega < \omega_{AR}$ above ϵ_{ARstab} . Note that the standard WNL zig-zag threshold ϵ_{ZZ}^s (49) [$\Gamma_G = \Gamma_\varphi = 0$ in Eq. (47c)], which diverges at $\omega \simeq 1.23$, is totally misleading. The results of the Galerkin computations [15] for the lines ϵ_{ZZ} (diamonds) and ϵ_{ARstab} (squares) are included.

tant at high ω where R gets large. Thus the standard zig-zag threshold ϵ_{ZZ}^s diverges at $\omega_{CD}=1.23$ (Fig. 6) in distinct contradiction to the experiments as well as to the Galerkin calculations which have shown the existence of a zig-zag instability up to $\omega_{AR}\approx 2.5$ [15,16].

C. Stability of normal rolls: Secondary zig-zag mechanism

By inclusion of the higher-order terms Γ_φ and Γ_G in Eq. (47), the zig-zag threshold ϵ_{ZZ}^s (49) is modified to

$$\epsilon_{ZZ}^s = \frac{r_2}{d_3}, \quad \text{with}$$

$$d_3 = \frac{1}{2} \left(d_2 + \frac{\Gamma_\varphi}{|\sigma_T|} r_2 + \sqrt{\left(d_2 - \frac{\Gamma_\varphi}{|\sigma_T|} r_2 \right)^2 + 8 \frac{\gamma' \delta\Gamma}{|\sigma_T|} r_2} \right), \quad (52a)$$

$$\delta\Gamma = \frac{s_1}{\nu_b} \Gamma_G - \frac{b_1}{|\sigma_T|} \Gamma_\varphi. \quad (52b)$$

If only Γ_φ is kept, then $\delta\Gamma$ is negative and the argument of the square root is usually negative (except in EC for ω very close to ω_L), i.e., the divergence of the zig-zag threshold persists [it is even more dramatic than with Eq. (49), e.g., it occurs now at $\omega_{CD}=0.9$ in EC]. Indeed, the term $\Gamma_\varphi |A|^2 \varphi$ in Eq. (47b) reduces the damping of φ : it thus produces the normal \rightarrow abnormal roll instability, but it also enhances the stabilizing influence of the twist dynamics on the zig-zag instability. On the contrary, keeping only the contribution of Γ_G in Eq. (52) yields a positive $\delta\Gamma$ since Γ_G turns out to be always positive. Then d_3 reduces to

$$d_3 \approx \frac{1}{2} \left(d_2 + \sqrt{d_2^2 + 8 \frac{\gamma' \delta\Gamma}{|\sigma_T|} r_2} \right), \quad (53)$$

which stays positive finite even when $d_2 \rightarrow -\infty$, i.e., even when the WNL zig-zag threshold (49) diverges totally. The exact zig-zag threshold (52a) is shown in Fig. 6 for EC [46]. The first correction to the standard WNL threshold ϵ_{ZZ}^s can be calculated analytically: for $\omega \rightarrow \omega_L$ and $r_2 \rightarrow 0^+$, $\epsilon_{ZZ}^s \rightarrow 0^+$, one finds

$$\epsilon_{ZZ} = \epsilon_{ZZ}^s - \frac{2\gamma'}{|\sigma_T| d_2} \delta\Gamma (\epsilon_{ZZ}^s)^2 + O((\epsilon_{ZZ}^s)^3),$$

where, for EC, the prefactor of $(\epsilon_{ZZ}^s)^2$ is -40 . Thus, whereas the slope of the zig-zag threshold at the Lifshitz point is not changed as compared with the standard WNL analysis, the domain of validity of the standard WNL analysis appears to be very limited. The zig-zag threshold ϵ_{ZZ} (52a) increases with frequency essentially because of a strong increase of r_2 and b_1 with ω . Eventually ϵ_{ZZ} meets the abnormal-roll line $\epsilon_{AR} = |\sigma_T|/\Gamma_\varphi$ at a crossover frequency ω_{AR} where $d_3 = r_2/\epsilon_{AR} = r_2 \Gamma_\varphi / |\sigma_T|$; according to Eq. (52a), $\delta\Gamma$ vanishes at the crossover point, $\delta\Gamma > 0$ for $\omega < \omega_{AR}$, $\delta\Gamma < 0$ for $\omega > \omega_{AR}$. The competition between the zig-zag and the abnormal-roll instabilities appears therefore to be controlled

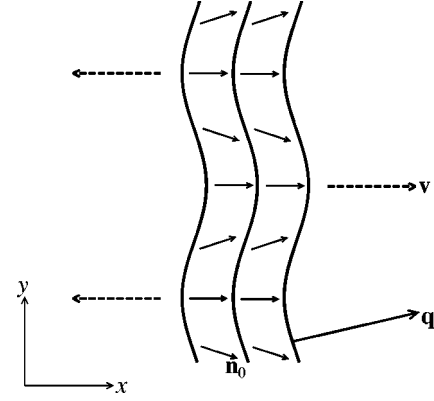


FIG. 7. Sketch of the mechanisms driving the zig-zag instability of normal rolls. The thick lines represent slightly undulated rolls, i.e., with a modulated local wave vector \mathbf{q} [see Eq. (50a)]. The ensuing roll curvature produces a mean flow \mathbf{v} (dashed arrows) which in turn advects the rolls and reinforces the undulations. In a secondary mechanism, the undulations generate a splay-twist modulation of the in-plane director \mathbf{n}_0 (small arrows inside the rolls), which in turn strongly reinforces, via a kind of “flow focusing,” the mean-flow.

by a balance between the Γ_G effects mainly responsible for the zig-zag instability (it occurs first if $\delta\Gamma > 0$) and the Γ_φ effects mainly responsible for the abnormal-roll instability (it occurs first if $\delta\Gamma < 0$). More quantitatively, for EC, our extended WNL computations reproduce the results of the Galerkin computations (compare Fig. 6 to Fig. 3 of [15]) very well at small ϵ , whereas for $\epsilon \gtrsim 0.07$ our values of ϵ_{ZZ} become slightly too small; thus we find the crossover point at $\omega_{AR} = 2.9$ instead of $\omega_{AR} = 2.4$ from the Galerkin computations. This agreement is satisfactory, and our analysis has the advantage of allowing for analytic modeling. For instance, by adjusting r_2 and b_1 , using otherwise the coefficients of Table III, one can perfectly reproduce the results of the full numerical calculation. Such an adjustment could possibly be used also for modeling experimental results (see also Sec. V D).

The new zig-zag mechanism expressed by the Γ_G effect can be understood by inspecting the corrections to the perturbation fields. Without Γ_φ , one finds that the roll (50a) and twist perturbations (50b) are unchanged, whereas the horizontal velocity (51) is modified according to

$$v_x \approx aA \frac{1}{\nu_b} \left(q_4 + \frac{\gamma'}{|\sigma_T|} \Gamma_G A^2 \right) p^2 \sin(py) P_1(z). \quad (54)$$

Thus the reinforcement of the zig-zag instability due to the Γ_G term is a three-step procedure (Fig. 7). First, the roll curvature induces the splay-twist modulation (50b). Second, this splay-twist modulation reinforces the mean flow already induced by the roll curvature (term $\propto q_4$ in v_x). Third, this mean flow (as known already from the standard mechanism) reinforces the roll curvature. We find that in EC and in ATC the dominant nonlinearities in Γ_G are contributions from the viscous terms in the v_x equation $\frac{1}{2}[(\alpha_5 - \alpha_2)(\partial_z v_x^f) n_z(\partial_y n_y) + (\alpha_5 + \alpha_2)(\partial_z v_z) n_z(\partial_y n_y)]$, which signifies a kind of “velocity focusing” associated with the long-wavelength splay term $\partial_y n_y$ (Fig. 7). It would be interesting to confirm this mechanism experimentally by optical

observations of the in-plane director: this should reveal, at the onset of the zig-zag instability, the splay-twist modulation shown in Fig. 7.

D. Restabilization of abnormal rolls at higher ϵ

In the parameter region where the normal rolls are first destabilized by the zig-zag instability (case $\omega < \omega_{AR}$ in EC, usual case in ATC), abnormal-roll solutions nevertheless exist for $\epsilon > \epsilon_{AR} > \epsilon_{ZZ}$. For symmetry reasons it seems clear that a sufficiently large rotation of the in-plane director will render these abnormal rolls stiff against long-wavelength zig-zag perturbations where the resonant interaction between the two modulation modes at $\pm p\hat{y}$ is important. A stability analysis of Eq. (47) does reveal the existence of a third stability boundary $\epsilon_{ARstab} > \epsilon_{AR} > \epsilon_{ZZ}$ where the zig-zag modulations of the abnormal-roll solutions are damped out. The $y \mapsto -y$ symmetry in Eq. (47) is broken by the b_2 and β terms in the A equation (47a), the terms g_φ and Γ_φ in the φ equation (47b), and the term Γ_G in the mean-flow equation (47c). The coefficients b_2 and g_φ seem to play no important role since their suppression only changes slightly (by less than 2%) the value of ϵ_{ARstab} . Assuming therefore $b_2 = g_\varphi = 0$ in Eq. (47), one obtains the following approximate formula:

$$\frac{\epsilon_{ARstab}}{\epsilon_{AR}} - 1 \approx \delta\Gamma \frac{\gamma'}{d_4}, \quad \text{with}$$

$$d_4 = \frac{\Gamma_\varphi}{2} \left[\frac{\Gamma_\varphi}{|\sigma_T|} r_2 - d_2 + 2\gamma' \frac{\delta\Gamma}{\Gamma_\varphi} \right. \\ \left. + \sqrt{\left(\frac{\Gamma_\varphi}{|\sigma_T|} r_2 - d_2 + 2\gamma' \frac{\delta\Gamma}{\Gamma_\varphi} \right)^2 - 4e_3 \gamma' \frac{\delta\Gamma}{\Gamma_\varphi}} \right]. \quad (55)$$

This shows clearly that the lines ϵ_{ZZ} , ϵ_{AR} , and ϵ_{ARstab} must meet at the crossover point $\delta\Gamma = 0$ in EC. An expansion of Eqs. (52a) and (55) in the vicinity of this point ($\omega \rightarrow \omega_{AR}^-$ in EC) yields a relation between their slopes:

$$\left(\frac{\epsilon_{ARstab}}{\epsilon_{AR}} - 1 \right) \sim -2 \left(\frac{\epsilon_{ZZ}}{\epsilon_{AR}} - 1 \right) \sim \frac{\gamma'}{\Gamma_\varphi (r_2 / \epsilon_{AR} - d_2)} \delta\Gamma. \quad (56)$$

This constraint on the slopes of the lines $\epsilon_{ARstab}(\omega)$ and $\epsilon_{ZZ}(\omega)$ at the crossover point could be easily tested experimentally [47]. Here we predict $\epsilon_{AR} \approx 0.076 - 0.030\delta\omega$, $\epsilon_{ARstab}/\epsilon_{AR} - 1 \approx -0.19\delta\omega$ or equivalently $\epsilon_{ARstab} \approx 0.076 - 0.044\delta\omega$ for $\delta\omega = \omega - \omega_{AR} = O(1)$, with frequencies in units of τ_{CD}^{-1} . The line $\epsilon_{ARstab}(\omega)$ calculated without approximations is shown in Fig. 6 for EC and matches roughly the numerical results [15] for not too small ω . However, $\epsilon_{ARstab}(\omega)$ increases too steeply with decreasing ω in contrast with the full numerical results (see the squares in Fig. 6 and Fig. 3 of [15]). Indeed at low frequencies, very high amplitudes are attained for $\epsilon \approx 0.15$ (Sec. IV B 2) and the WNL perturbation approach is no longer justified.

Note that only a few parameters determine the position of the bifurcation lines ϵ_{ZZ} (52a), ϵ_{AR} and ϵ_{ARstab} (55): the linear coefficients r_2 , e_3 , and σ_T and the nonlinear coefficients

d_2 , Γ_φ , and $\delta\Gamma' = \gamma' \delta\Gamma/\Gamma_\varphi$. The linear coefficients should be relatively easy to determine in experiments. Measurements of ϵ_{AR} for $\omega > \omega_{AR}$, together with an extrapolation in the domain $\omega < \omega_{AR}$ (observe that $\epsilon'_{AR}(\omega)$ is very smooth [Fig. 2(b)]), would then yield the values of Γ_φ . The remaining coefficients d_2 and $\delta\Gamma'$ could then be determined by fitting the expressions (52a) and (55) of ϵ_{ZZ} and ϵ_{ARstab} to the measured values of the zig-zag and abnormal-roll restabilization thresholds.

VI. NONLINEAR BIMODAL SOLUTIONS

Abnormal or oblique rolls of wave vector \mathbf{q} are stable against long-wavelength perturbations in an intermediate ϵ range; e.g., in EC the abnormal rolls for $\epsilon \gtrsim \epsilon_{ARstab}$. Experiments (see, e.g., [20,19]), as well as numerical simulations [27] or WNL analyses (see, e.g., [26]), have shown that they are rather destabilized in this regime by a short-wavelength mode of wave vector \mathbf{k} leading to a bimodal structure. Amplitude equations modeling such instabilities can be derived with calculations similar to those of Sec. IV A, where we add a secondary roll mode to the basic ansatz for the extended WNL solutions (25), now

$$V = V_{\mathcal{A}} + V_{\perp} = [A V_1(\mathbf{q}) + B V_1(\mathbf{k}) + \text{c.c.}] + \varphi V_T + V_{\perp}. \quad (57)$$

One should realize that since we leave the ‘‘very small ϵ ’’ region, no quantitative results are to be expected in general. Nevertheless, we will obtain in some regimes (EC at high ω) semiquantitative results, and, more importantly, qualitative results concerning the origin of the bimodal instability and the further stability of the bimodal solutions themselves (which had never been studied theoretically).

A. Bimodal-twist amplitude equations

With the scheme of Appendix B and calculations performed at $R = R_0(\mathbf{q})$ in order to avoid R dependencies of the nonlinear coefficients in the amplitude equations, we get from Eq. (57)

$$\partial_t A = \left(\frac{\epsilon - \epsilon_0(\mathbf{q})}{\tau_{\mathbf{q}}} - g_{\mathbf{q}} |A|^2 + \beta_2(\mathbf{q}) \varphi - \beta_3(\mathbf{q}) \varphi^2 \right) A \\ - g_{\mathbf{kq}} |B|^2 A, \\ \partial_t \varphi = [\sigma_T - g_\varphi \varphi^2 + \Gamma(\mathbf{q}) |A|^2 + \Gamma(\mathbf{k}) |B|^2] \varphi \\ - \gamma(\mathbf{q}) |A|^2 - \gamma(\mathbf{k}) |B|^2, \\ \partial_t B = \left(\frac{\epsilon - \epsilon_0(\mathbf{k})}{\tau_{\mathbf{k}}} - g_{\mathbf{k}} |B|^2 + \beta_2(\mathbf{k}) \varphi - \beta_3(\mathbf{k}) \varphi^2 \right) B \\ - g_{\mathbf{kq}} |A|^2 B. \quad (58)$$

The coupling coefficient $g_{\mathbf{kq}}$ is

$$g_{\mathbf{kq}} = - \langle U_1(\mathbf{k}), N_2(V_1(-\mathbf{q}) | V_2(\mathbf{q}, \mathbf{k})) \\ + N_2(V_1(\mathbf{q}) | V_2(-\mathbf{q}, \mathbf{k})) + N_2(V_2(\mathbf{q}, -\mathbf{q}) | V_1(\mathbf{k})) \\ + N_3(V_1(\mathbf{q}) | V_1(-\mathbf{q}) | V_1(\mathbf{k})) \rangle, \quad (59)$$

TABLE V. Coefficients of the bimodal-twist amplitude equations (58), in ATC for an experimental zig wave vector \mathbf{q} and the corresponding dual wave vector \mathbf{k} (see text).

$\tau_{\mathbf{q}}$	$\epsilon_0(\mathbf{q})$	$g_{\mathbf{q}}$	$\beta_2(\mathbf{q})$	$\beta_3(\mathbf{q})$	$g_{\mathbf{kq}}$	$\tau_{\mathbf{k}}$	$\epsilon_0(\mathbf{k})$	$g_{\mathbf{k}}$	$\beta_2(\mathbf{k})$	$\beta_3(\mathbf{k})$	$g_{\mathbf{qk}}$
267	0.013	0.0054	0.00010	0.0011	0.013	431	0.16	0.0024	-0.0010	0.0017	0.0025
$\sigma_{\mathcal{T}}$	g_{φ}	$\Gamma(\mathbf{q})$	$\Gamma(\mathbf{k})$	$\gamma(\mathbf{q})$	$\gamma(\mathbf{k})$						
-0.00081	0.00010	0.0077	0.0034	0.0014	-0.0048						

where the second harmonics are defined as in Eq. (28), e.g.,

$$V_2(\mathbf{q}, \mathbf{k}) = -L_{R_0(\mathbf{q})}^{-1} \cdot N_2(V_1(\mathbf{q})|V_1(\mathbf{k})). \quad (60)$$

B. Bimodal instability

Consider a primary solution of the zig type characterized by a wave vector $\mathbf{q} = q\hat{\mathbf{x}} + p\hat{\mathbf{y}}$ with $p \geq 0$, an amplitude $A = A(\mathbf{q}; \epsilon)$, and an in-plane director rotation $\varphi = \varphi(\mathbf{q}; \epsilon) < 0$ (this can include both abnormal and oblique-roll solutions, see the discussion at the end of Sec. IV C). The growth rate of the short-wavelength perturbation of wave vector \mathbf{k} deduced from Eq. (58) is

$$\sigma_{\text{BV}}(\mathbf{q}; \mathbf{k}; \epsilon) = \frac{\partial_{\epsilon} B}{B} = \frac{\epsilon - \epsilon_0(\mathbf{k})}{\tau_{\mathbf{k}}} + \beta_2(\mathbf{k}) \varphi - \beta_3(\mathbf{k}) \varphi^2 - g_{\mathbf{qk}} |A|^2. \quad (61)$$

In EC and in ATC, σ_{BV} first becomes positive at $\epsilon = \epsilon_{\text{BV}}$ for a certain wave vector \mathbf{k} (the ‘‘dual’’ of \mathbf{q}) of the zag type ($k_y < 0$). This selection can be heuristically understood by noticing that the growth rate $\sigma_{\text{BV}}(\mathbf{q}; \mathbf{k}; \epsilon)$ at the dual \mathbf{k} is much larger than $\sigma_{\text{BV}}(\mathbf{q}; \mathbf{k}'; \epsilon)$ for a \mathbf{k}' in the zig region, e.g., at $\mathbf{k}' = S(\mathbf{k})$. Since the coefficients $\epsilon_0(\mathbf{k})$, $\tau_{\mathbf{k}}$, and $\beta_3(\mathbf{k})$ are unchanged under the application of S , and $g_{\mathbf{qk}}$ is only slightly modified [52], one obtains $\sigma_{\text{BV}}(\mathbf{q}; \mathbf{k}; \epsilon) \approx \sigma_{\text{BV}}(\mathbf{q}; S(\mathbf{k}); \epsilon) + 2\beta_2(\mathbf{k})\varphi$: the fact that $\beta_2(\mathbf{k})$ is large and negative in the zag region (and $\varphi < 0$) explains the selection. Typically $\mathbf{k} \neq S(\mathbf{q})$ so the resulting unsymmetric bimodal is of the ‘‘bimodal varicose’’ type [14].

In EC for the abnormal rolls at $q = q_c$, we find values of ϵ_{BV} that are too small at low ω . The reason is that $|\varphi(\mathbf{q}; \epsilon)|$ gets too large when compared with the Galerkin computations (Sec. IV B 2). However, the position of the dual is qualitatively correct. For instance, at $\omega_{\text{CD}} = 1$ we find $|\mathbf{k}| = 1.18q_c$, $\arg \mathbf{k} = -67^\circ$ [48], to be compared with $|\mathbf{k}| = 1.01q_c$, $\arg \mathbf{k} = -61^\circ$ from the Galerkin computations. At higher ω , since the abnormal-roll solutions are closer to the numerical Galerkin solutions (Sec. IV B 2 and Fig. 3), both ϵ_{BV} and \mathbf{k} agree reasonably well with the ones from the Galerkin computations. For instance, at $\omega_{\text{CD}} = 2.4$, we find $\epsilon_{\text{BV}} = 0.186$, $|\mathbf{k}| = 0.98q_c$, $\arg \mathbf{k} = -33^\circ$ [49], to be compared with $\epsilon_{\text{BV}} = 0.183$, $|\mathbf{k}| = 0.95q_c$, $\arg \mathbf{k} = -26^\circ$ from the Galerkin computations. We mention that the bifurcation to the bimodal varicose has also been evidenced recently in EC of the nematic I52 at high electric conductivity [50].

In ATC, for the primary zig mode $\mathbf{q} = 1.07q_c(\hat{\mathbf{x}} \cos 8^\circ + \hat{\mathbf{y}} \sin 8^\circ)$, we find $\epsilon_{\text{BV}} = 0.176$, $|\mathbf{k}| = 0.86|\mathbf{q}|$, $\arg \mathbf{k} = -32^\circ$, in qualitative agreement with the experimental observations

[14]. The corresponding coefficients (Table V) will be used in Sec. VI C for numerical simulations of the system (58).

For all these bimodal instabilities, the leading positive contribution to $\sigma_{\text{BV}}(\mathbf{q}; \mathbf{k}; \epsilon_{\text{BV}})$ (61) is always $\beta_2(\mathbf{k})\varphi$, whereas the (typically negative) contribution of $\beta_3(\mathbf{k})\varphi^2$ is smaller in magnitude [51]. This proves that the director rotation ($\varphi < 0$) in the primary rolls is the main cause for the excitation of a mode with wave vector in the zag region. This holds for primary abnormal ($p = 0$) or oblique rolls ($p > 0$) and generalizes the mechanism identified in [26] for ATC, which appears to be also valid for EC. Finally, note that this mechanism can also be understood from the frustration introduced in Sec. IV D: the director rotation in zigs being driven by (M2) and the subsequent excitation of a zag roll by (M1).

C. Bimodal-twist solutions—Hopf bifurcation

The main advantage of the model system (58) is that approximate bimodal solutions can be calculated, and that their stability can now be studied. Let $A, B \neq 0$, then Eq. (58) yields a cubic equation for φ after the elimination of $|A|^2$ and $|B|^2$. For primary abnormal rolls, there exists a unique stable solution for $\epsilon_{\text{BV}} < \epsilon < \epsilon_{\text{Hopf}}$ (see below for ϵ_{Hopf}), and the bimodal bifurcation is supercritical. For primary oblique rolls, we find a stable solution in a slightly larger ϵ domain, $\epsilon_{\text{BV}} - \delta\epsilon_{\text{BV}} < \epsilon < \epsilon_{\text{Hopf}}$: the bimodal bifurcation is, in fact, slightly subcritical. With the parameters of Table V, $\delta\epsilon_{\text{BV}} = 0.002 \ll 1$: the corresponding hysteresis appears to be impossible to observe experimentally. However, the jumps in B and φ at $\epsilon = \epsilon_{\text{BV}}$ are not small and might be observable (see the left side of Fig. 8). Note that after the bimodal transition, φ increases steeply owing to the term $-\gamma(\mathbf{k})|B|^2$ in the φ equation, where $\gamma(\mathbf{k}) < 0$ since \mathbf{k} is zag. The stability of the bimodal branch against perturbations in A, B , and φ can be studied by linearization of Eq. (58). One always finds a Hopf bifurcation at sufficiently large $\epsilon > \epsilon_{\text{Hopf}}$. With the coefficients of Table V, $\epsilon_{\text{Hopf}} = 0.22$, and the development of the Hopf bifurcation is shown, on the right side of Fig. 8, by a time-forward simulation of Eq. (58) after a jump from $\epsilon = 0.22$ to 0.228. The two amplitudes oscillate roughly out of phase, as observed experimentally in the oscillating bimodals (see, e.g., [19] or Fig. 12 of [20]). The calculated period of these *bimodal-twist oscillations* is $T = 48\tau_{\mathbf{q}} = 44\tau$, which is not too far from the periods measured experimentally, $T \approx 15\tau$ [20]. The existence of these oscillations is robust against changes in the parameters of Table V, provided that their sign is left unchanged.

In order to analyze the origin of these oscillations, we now focus on the simpler case of a symmetric bimodal $\mathbf{k} = S(\mathbf{q})$. Such symmetric bimodals are often observed at

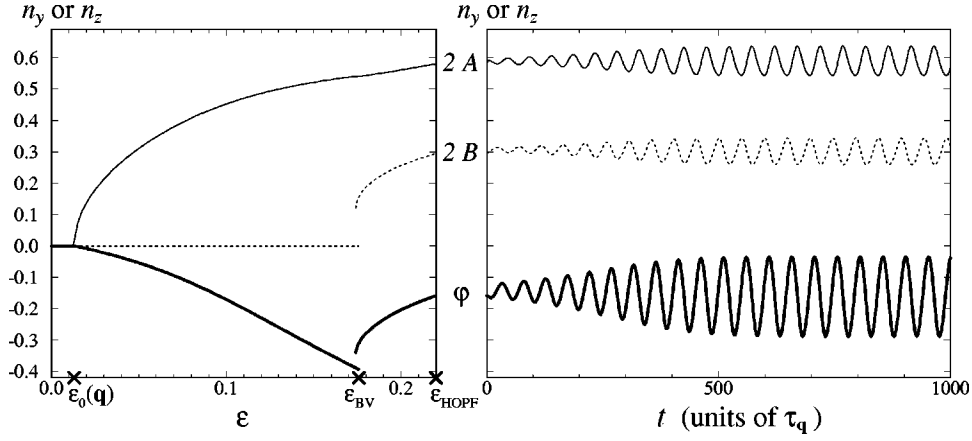


FIG. 8. Solutions of the coupled amplitude equations (58) modeling the interactions between two roll modes of wave vector \mathbf{q} (zig) and \mathbf{k} (zag) and the homogeneous twist mode. The coefficients of Table V have been used, and the roll amplitudes A (thin line), B (dotted line) have been multiplied by 2 in order to display the leading amplitudes of the n_z field in Eq. (57), $n_z = -[2A \sin \mathbf{q} \cdot \mathbf{r} + 2B \sin \mathbf{k} \cdot \mathbf{r}]S_1(z) + \text{h.o.t.}$ The amplitude φ (thick line) determines to lowest order the angle between the average in-plane director and $\hat{\mathbf{x}}$. Left panel: stationary solutions obtained in the “low ϵ ” regime. For $\epsilon_0(\mathbf{q}) < \epsilon < \epsilon_{\text{BV}}$, one has monomode solutions ($A \neq 0, B = 0$). At $\epsilon = \epsilon_{\text{BV}}$, a subcritical bifurcation towards a bimodal ($A, B \neq 0$) occurs; only the stable bimodal solutions are then shown. Right panel: behavior just above the threshold of the Hopf bifurcation ϵ_{Hopf} . After a jump from $\epsilon = 0.22 < \epsilon_{\text{Hopf}}$ to $\epsilon = 0.228 > \epsilon_{\text{Hopf}}$, regular out of phase oscillations of A and B develop, which are mediated by an oscillation of the in-plane director.

rather high values of the control parameter in EC and in ATC after an evolution with R of the wave vectors of the bimodal varicose [53]. In this symmetric case, assuming that Eq. (58) is still valid to describe the dynamics of the system, an analytic calculation of the Hopf threshold becomes tractable. Since the phases of A and B are not coupled by the system (58), we can consider these amplitudes to be real without loss of generality. After some simple rescalings, Eq. (58) takes the simpler form

$$\begin{aligned} \partial_t A &= (\epsilon - A^2 + \beta_2 \varphi - \beta_3 \varphi^2)A - gB^2 A, \\ \partial_t \varphi &= [\sigma_T - g_\varphi \varphi^2 + \Gamma(A^2 + B^2)]\varphi + \gamma(B^2 - A^2), \\ \partial_t B &= (\epsilon - B^2 - \beta_2 \varphi - \beta_3 \varphi^2)B - gA^2 B, \end{aligned} \quad (62)$$

where $g = g_{\mathbf{qS}(\mathbf{q})} = g_{S(\mathbf{q})\mathbf{q}}, \beta_2 = \beta_2(\mathbf{q}) = -\beta_2(S(\mathbf{q})) > 0, \gamma = \gamma(\mathbf{q}) = -\gamma(S(\mathbf{q})) > 0$. For $g > -1$, this system admits stationary bimodal solutions given by $A = B = \sqrt{\epsilon/(1+g)} = \sqrt{\epsilon'}, \varphi = 0$. If we perturb these solutions according to

$$A = \sqrt{\epsilon'} + a, \quad B = \sqrt{\epsilon'} + b, \quad \varphi = 0 + \varphi,$$

it turns out that the modes $a + b$ and $b - a$ are decoupled, and that the former is always damped. The perturbation system then reduces to

$$\begin{aligned} \partial_t (b - a) &= -2\epsilon'(1 - g)(b - a) - 2\beta_2 \sqrt{\epsilon'} \varphi, \\ \partial_t \varphi &= 2\gamma \sqrt{\epsilon'} (b - a) + (\sigma_T + 2\Gamma \epsilon') \varphi. \end{aligned} \quad (63)$$

If we suppose that a fluctuation in the roll amplitudes favors the zag mode B , then the director will avoid the stronger gradients along the zag wave vector by rotating towards the zig: φ then becomes positive due to the γ term in the second equation. But this rotation will then favor A , at the expense of B , due to the β_2 term in the first equation: $b - a$ will now decrease. If the $\Gamma \epsilon'$ term in Eq. (63) is sufficiently large to

overcompensate the damping of the modes $b - a$ and φ , i.e., if the trace of the matrix (63) is positive:

$$2\epsilon'(\Gamma + g - 1) + \sigma_T > 0 \Leftrightarrow \Gamma > 1 - g,$$

$$\epsilon' > \epsilon'_{\text{Hopf}} = \frac{1}{2} \frac{|\sigma_T|}{\Gamma + g - 1}, \quad (64)$$

$b - a$ will even change sign and thus make the director rotate in the opposite direction (now towards the zag). Thus a Hopf bifurcation will occur, under the additional conditions that the discriminant of the system (63) is negative at $\epsilon' = \epsilon'_{\text{Hopf}}$:

$$\Delta = \frac{4|\sigma_T|}{(\Gamma + g - 1)^2} [|\sigma_T|(g - 1)^2 - 2\beta_2 \gamma(\Gamma + g - 1)] < 0, \quad (65)$$

and that a stationary instability does not occur before:

$$|\sigma_T|(g - 1) - 2\beta_2 \gamma < 0. \quad (66)$$

These conditions are typically fulfilled since $|\sigma_T|$ is small whereas the product $\beta_2 \gamma$ is large in oblique rolls. This, together with the fact that the instability condition (64) is easy to realize with the large Γ expected for nematic convection, proves that the bimodal-twist oscillations are generic, as expected from the experiments. The leading mechanism, clearly linked to the fact that $\beta_2(\mathbf{q})$ and $\gamma(\mathbf{q})$ change sign when passing from the zig to the zag, is sketched in Fig. 9. It can be interpreted in terms of the director-wave-vector frustration introduced in Sec. IV D. Indeed, if a fluctuation favors one roll amplitude in the bimodal, according to (M2) the director will be pushed away from the wave vector of this roll mode. Thus the director will approach the wave vector of the other roll mode, which will be reinforced according to (M1), and so on (Fig. 9).

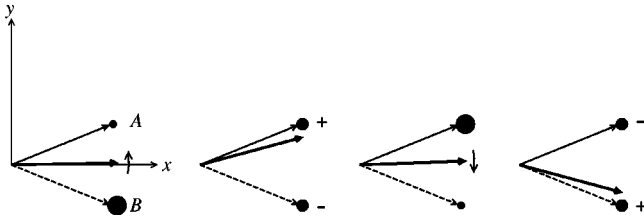


FIG. 9. Sketch of the mechanism driving the bimodal-twist oscillations. The thin arrows show the zig (continuous line) and the zag (dashed line) wave vectors of the two roll modes in the bimodal. The magnitude of the corresponding amplitudes A and B is symbolized by the size of the Fourier spots attached to these wave vectors. The in-plane director \mathbf{n}_0 , such that $\mathbf{n}_0 \cdot \hat{\mathbf{y}} = \varphi$, is drawn with the thick arrow. The four elementary steps during one oscillation are shown side by side. The torque $\propto \alpha_2$ exerted by the rolls on the director is sketched with the vertical arrows, and the positive (negative) feedback from the director to the roll amplitudes is indicated with the $+$ ($-$).

In fact, secondary indirect mechanisms for the feedbacks $\varphi \leftrightarrow A$ implied in this instability loop are provided by the interactions $\varphi \leftrightarrow B$ and $B \leftrightarrow A$. For instance, an increase of φ leads to an increase of A (second step of Fig. 9) due to the term in $\beta_2(\mathbf{q}) > 0$ in Eq. (58), but also because it first produces a decrease of B [due to the terms in $\beta_2(\mathbf{k}) < 0, \beta_3(\mathbf{k}) > 0$] which then drives an increase of A (due to the term in $g_{\mathbf{kq}} > 0$). In a similar way, an increase of A drives a decrease of φ (third step of Fig. 9) directly due to the $\gamma(\mathbf{q})$ term [$\gamma(\mathbf{q}) > 0$], or indirectly, via a decrease of B , due to the $g_{\mathbf{qk}}$ and $\gamma(\mathbf{k})$ terms [$g_{\mathbf{qk}} > 0$ and $\gamma(\mathbf{k}) < 0$]. An important consequence of these indirect mechanisms is that the oscillations also develop in a bimodal constructed on primary abnormal rolls for which $\beta_2(\mathbf{q}) = \gamma(\mathbf{q}) = 0$. Indeed, simulations of Eq. (58) with a set of coefficients calculated in EC of N5 at $\omega_{\text{CD}} = 2.4$ for the bimodal constructed on the abnormal rolls at $q = q_c$ show the same sequence as in Fig. 8, now with $\epsilon_{\text{BV}} = 0.186$ and $\epsilon_{\text{Hopf}} = 0.24$. Of course, these oscillations disappear if $g_{\mathbf{qk}}$ or $g_{\mathbf{kq}}$ are set negative.

VII. CONCLUSION

A minimal description of planar nematic convection has been obtained which captures the generic bifurcation sequences known experimentally. It is based on a systematic WNL analysis where the active mode basis has been extended: besides the standard roll modes, “slow modes” consisting of homogeneous or quasihomogeneous twist modes of the director have also been included. The evolution equations coupling the corresponding order parameter φ with the roll amplitudes A (or B) and with the mean-flow amplitude G [Eqs. (29), (47), and (58)] have allowed a quantitative description of the first bifurcations at small ϵ (see, e.g., Fig. 11) and a qualitative description of the subsequent bifurcations at higher ϵ (see, e.g., Fig. 8). Due to the semianalytic nature of the calculations, the dominant nonlinear microscopic mechanisms could be singled out. This gives indications concerning the behavior of nematics with other material parameters. In general, the interactions between the twist and the roll amplitudes appear to be ruled by a principle that we have termed “director–wave-vector frustration”: the charge- and heat-focusing mechanisms both favor the in-plane director

almost parallel to the roll wave vectors, whereas the viscous torques always push it away (Sec. IV D). This explains the close analogy between electroconvection and thermoconvection.

A systematic calculation of the order-parameter equations as presented here might also provide a better understanding of the microscopic mechanisms for other systems where slow modes play an important role. Examples are binary fluid convection with slow concentration modes [54] or nematic electroconvection in the presence of weak-electrolyte effects, in which slow charge modes allegedly drive the formation of the surprising “worms” [55].

We hope that our results will stimulate new experimental studies of electroconvection and thermoconvection, where some features characteristic of the roll-twist-mean-flow interactions could be evidenced: e.g., the dynamics at the zig-zag instability (Fig. 7), the in-plane director oscillations underlying the bimodal oscillations (Fig. 9), or the change in the trajectory trace quoted in Appendix C. Since all the basic structures and instability lines are now well understood, this work also establishes a starting point for a systematic theoretical study of more complicated nonperiodic patterns. For instance, the rich dynamics of structures with point defects or walls [56] needs further investigation. In particular, the spatiotemporal chaos observed under certain experimental conditions might be better described and understood from envelope equations of a type similar to Eqs. (47). For that purpose, an extension of these equations to the case of a general spatial dependence (both ∂_y and $\partial_x \neq 0$) is under way. It would also be interesting to reanalyze the phase dynamics in the oscillating bimodals, which had been previously described on the basis of phenomenological models [57].

We note finally the similarities with homeotropic nematic electroconvection, where one sets $\mathbf{n} = \hat{\mathbf{z}}$ at the plates and therefore the rotational symmetry around z is initially not broken. Convection sets in after an electric Fréedericksz transition where the in-plane director orientation is selected, and the associated Goldstone mode plays a role analogous to our twist mode in planar convection. In fact, the first experiments pointing to the existence of abnormal rolls were performed in homeotropic electroconvection [58], and the amplitude equations derived for this system in [30] are similar to our amplitude equations in their simplest form [59]. In the presence of a planar magnetic field, the homeotropic system becomes anisotropic. Galerkin computations [60] and experiments [61] have then shown sequences of bifurcations identical to the ones observed in the planar case. It would be interesting to systematically calculate the corresponding order-parameter equations, particularly to elucidate the role of the mean flow in this homeotropic case.

ACKNOWLEDGMENTS

We thank L. Kramer, A. G. Rossberg, and M. Treiber for very fruitful discussions, and D. Egolf for carefully reading the manuscript. Financial support by the Deutsche Forschungsgemeinschaft (Grant No. DFG-Kr690/4-4), and the TMR network “Patterns, Noise and Chaos” (Grant No. FMRX-CT96-0085), is gratefully acknowledged.

APPENDIX A: LINEAR EQUATIONS FOR THE FOCUSING MECHANISMS

The focusing mechanisms and the analogy between EC and ATC become clearer by inspection of the corresponding dimensionless linear equations. In EC, the evolution of the scalar field, the electric potential ϕ , is governed by Eq. (5),

$$\begin{aligned} & -(\epsilon_{\perp}\nabla^2 + \epsilon_a\partial_x^2)\partial_t\phi + \epsilon_a\partial_t(E_{ac}\partial_x n_z) \\ & = Q(\sigma_{\perp}\nabla^2 + \sigma_a\partial_x^2)\phi - Q\sigma_a E_{ac}(\partial_x n_z), \end{aligned} \quad (\text{A1})$$

with $E_{ac} = \cos \omega t$. This equation presents the same kind of focusing terms ($\propto \partial_x n_z$) as the evolution equation for the temperature modulation θ in ATC which follows from Eq. (7),

$$\partial_t\theta = (\kappa_{\perp}\nabla^2 + \kappa_a\partial_x^2)\theta + Rv_z - R\kappa_a\partial_x n_z. \quad (\text{A2})$$

The evolution equation for n_z , deduced from Eq. (1), contains in both cases the same elastic and viscous terms,

$$\begin{aligned} \gamma_1\partial_t n_z &= (k_{33}\partial_x^2 + k_{22}\partial_y^2 + k_{11}\partial_z^2)n_z \\ &+ (k_{11} - k_{22})\partial_y\partial_z n_y - \alpha_2\partial_x v_z - \alpha_3\partial_z v_x + h'_z, \end{aligned} \quad (\text{A3})$$

with the dimensionless units for EC; the important term here is the viscous torque $\propto \partial_x v_z$. In EC additional electric terms come in,

$$h'_z = \epsilon_a R n_z - 2\epsilon_a R E_{ac}\partial_x\phi, \quad (\text{A4})$$

which are only important at high frequencies. Finally, the evolution equation for v_z , deduced from Eq. (3), is also rather similar for both systems,

$$\begin{aligned} \rho_m\partial_t v_z - \alpha_2\partial_t\partial_x n_z &= (\nu_c\partial_x^2 + \nu_a\partial_y^2 + \nu_a\partial_z^2)v_z \\ &+ \frac{1}{2}(\alpha_2 + \alpha_5)\partial_x\partial_z v_x + f_{\text{vol}}, \end{aligned} \quad (\text{A5})$$

with the dimensionless units for EC (for ATC one has only to change ρ_m into $1/Pr$), with the bulk force being given by the Coulomb force (6) in EC,

$$f_{\text{vol}} = \epsilon_a R \partial_x n_z - 2R E_{ac}(\epsilon_{\perp}\nabla^2 + \epsilon_a\partial_x^2)\phi, \quad (\text{A6})$$

and by the buoyancy force (8) in ATC,

$$f_{\text{vol}} = \theta. \quad (\text{A7})$$

APPENDIX B: EXTENDED WEAKLY NONLINEAR SCHEME

In this appendix we show how to calculate approximate WNL solutions of a problem of the form

$$D\partial_t V = LV + N_2(V, V) + N_3(V, V, V), \quad (\text{B1})$$

with the order-parameter approach. The main control parameter R (not recalled in order to simplify the notations) is fixed. The linear modes, the solutions of

$$\sigma(\mathbf{m})DV_1(\mathbf{m}) = LV_1(\mathbf{m}), \quad (\text{B2})$$

are indexed by a collection of numbers \mathbf{m} ; for instance, in the ‘‘extended layer’’ geometry, $\mathbf{m} = (\mathbf{q}, n)$ where \mathbf{q} is the horizontal wave vector and n indexes the vertical dependence (in z). These linear modes are assumed to form a basis in V space. With the help of a Hermitian scalar product in V space, $(U, V) \mapsto \langle U, V \rangle$, we define the adjoint linear operators D^\dagger and L^\dagger by $\langle U, D \cdot V \rangle = \langle D^\dagger \cdot U, V \rangle$, and the adjoint linear modes as the solutions of

$$\sigma(\mathbf{m})D^\dagger \cdot U_1(\mathbf{m}) = L^\dagger \cdot U_1(\mathbf{m}). \quad (\text{B3})$$

They can be normalized such that

$$\langle U_1(\mathbf{m}), DV_1(\mathbf{m}') \rangle = \delta(\mathbf{m} - \mathbf{m}'). \quad (\text{B4})$$

The growth rates $\sigma(\mathbf{m})$ are assumed real. We distinguish between the *active modes* of growth rate $\sigma(\mathbf{m}) > -c$ (which defines a domain \mathcal{A} in \mathbf{m} space) and the *passive modes* of growth rate $\sigma(\mathbf{m}) < -c$ (which defines a domain \mathcal{P} in \mathbf{m} space). Usually in the solutions of Eq. (B1) there is a clear separation between the growth rates of the excited active modes and the growth rates of the excited passive modes (see below), and therefore the exact value of c is not very important. We assume the existence of a primary instability:

$$\max_{\mathbf{m} \in \mathcal{A}} \sigma(\mathbf{m}) = \epsilon > 0, \quad (\text{B5})$$

with $\epsilon \ll c$. The orthogonality rule (B4) allows the definition of a projector onto the active mode space by

$$P_{\mathcal{A}}V = \sum_{\mathbf{m} \in \mathcal{A}} \langle U_1(\mathbf{m}), DV \rangle V_1(\mathbf{m}), \quad (\text{B6})$$

and onto the passive mode space by

$$(1 - P_{\mathcal{A}})V = \sum_{\mathbf{m}' \in \mathcal{P}} \langle U_1(\mathbf{m}'), DV \rangle V_1(\mathbf{m}'). \quad (\text{B7})$$

Thus a natural decomposition of possible approximate solutions of the evolution equation (B1) is

$$\begin{aligned} V &= V_{\mathcal{A}} + V_{\perp} \\ &= P_{\mathcal{A}}V + (1 - P_{\mathcal{A}})V \\ &= \sum_{\mathbf{m} \in \mathcal{A}} A(\mathbf{m})V_1(\mathbf{m}) + \sum_{\mathbf{m}' \in \mathcal{P}} B(\mathbf{m}')V_1(\mathbf{m}'). \end{aligned} \quad (\text{B8})$$

A mode $V_1(\mathbf{m})$ or $V_1(\mathbf{m}')$ is ‘‘excited’’ if the corresponding amplitude $A(\mathbf{m})$ or $B(\mathbf{m}')$ is nonzero; the $A(\mathbf{m})$ constitute, in fact, the ‘‘active amplitudes’’ or ‘‘order parameters’’ which will define the solution. In order to show this, we introduce the coprojector P'_A defined by

$$P'_A V = \sum_{\mathbf{m} \in \mathcal{A}} \langle U_1(\mathbf{m}), V \rangle D V_1(\mathbf{m}), \quad (\text{B9})$$

such that $P'_A D = D P'_A$ and $P'_A L = L P'_A$. The application of $(1 - P'_A)$ on Eq. (B1) then gives to lowest order

$$D \partial_t V_\perp = L V_\perp + (1 - P'_A) N_2(V_A, V_A), \quad (\text{B10})$$

which shows that if V_A is assumed to be of order A , V_\perp is of order A^2 . Moreover, the projection of Eq. (B10) onto $U_1(\mathbf{m}')$ gives

$$\partial_t B(\mathbf{m}') = \sigma(\mathbf{m}') B(\mathbf{m}') + \langle U_1(\mathbf{m}'), N_2(V_A, V_A) \rangle.$$

Assuming that ∂_t is of the order of the maximum growth rate of the active modes (B5), we get $\partial_t \ll |\sigma(\mathbf{m}')|$ and can therefore perform an *adiabatic elimination* of $B(\mathbf{m}')$,

$$B(\mathbf{m}') = - \frac{1}{\sigma(\mathbf{m}')} \langle U_1(\mathbf{m}'), N_2(V_A, V_A) \rangle, \quad (\text{B11})$$

or equivalently solve Eq. (B10) by

$$V_\perp = -L^{-1}(1 - P'_A) N_2(V_A, V_A). \quad (\text{B12})$$

The projection of Eq. (B1) onto the $U_1(\mathbf{m})$ gives the final active amplitude equations

$$\begin{aligned} \partial_t A(\mathbf{m}) = & \sigma(\mathbf{m}) A(\mathbf{m}) + \langle U_1(\mathbf{m}), N_2(V_A, V_A) + N_2(V_A | V_\perp) \\ & + N_3(V_A, V_A, V_A) \rangle, \end{aligned} \quad (\text{B13})$$

where we have introduced the notations (used in the rest of the paper for the cubic order)

$$N_2(a|b) = N_2(a, b) + N_2(b, a),$$

$$N_3(a|a|b) = N_3(a, a, b) + N_3(a, b, a) + N_3(b, a, a),$$

$$N_3(a|b|c) = N_3(a, b, c) + N_3(a, c, b) + N_3(b, a, c)$$

$$+ N_3(c, a, b) + N_3(b, c, a) + N_3(c, b, a).$$

$$(\text{B14})$$

In practice, often the eigenmodes (or the operators L and N_2) at the control parameter R are not used to calculate the nonlinear coefficients of the amplitude equations since this would introduce an R dependence of these coefficients. Instead, one uses, for instance, in convection the neutral roll modes $V_1(\mathbf{q}) := V_1(\mathbf{q}; R_0(\mathbf{q}))$ instead of $V_1(\mathbf{q}; R)$ or evaluates $L^{-1} = L_R^{-1}$ in Eq. (B12) at $R = R_0(\mathbf{q})$; clearly this introduces only small numerical corrections to the scheme. Note finally that the scalar product in our layer geometry is defined by

$$\begin{aligned} \langle U(z) e^{i\mathbf{q} \cdot \mathbf{r}}, V(z) e^{i\mathbf{q}' \cdot \mathbf{r}} \rangle \\ = \delta(\mathbf{q} - \mathbf{q}') \frac{2}{\pi} \int_{z=-\pi/2}^{z=\pi/2} U^*(z)^t V(z) dz. \end{aligned} \quad (\text{B15})$$

APPENDIX C: ANALYTIC APPROXIMATION OF THE NONLINEAR ROLL-TWIST COEFFICIENT Γ

In this appendix we use the lowest-order Galerkin expansion to give analytic approximations of the coefficient $\Gamma(\mathbf{q})$ (33) and to elucidate the corresponding mechanisms (at $\mathbf{q} = q_c \hat{\mathbf{x}}$). The contribution $\Gamma_3(\mathbf{q})$ of the cubic nonlinearities then reads

$$\gamma_1 \Gamma_3(\mathbf{q}) = \begin{cases} 2.21 |\alpha_2| q_c \tilde{f} \tilde{n}_z + 1.56 \alpha_3 q_c^3 \tilde{f} \tilde{n}_z + \frac{6(k_{33} - k_{22}) q_c^2 - 2k_{33} + k_{22}}{4} \tilde{n}_z^2 + \frac{3}{4} q_c R \epsilon_a [\tilde{n}_z (\tilde{\phi} + \tilde{\phi}^*) - 4q_c |\tilde{\phi}|^2] & \text{in EC} \\ 2.21 |\alpha_2| q_c \tilde{f} \tilde{n}_z + 1.56 \alpha_3 q_c^3 \tilde{f} \tilde{n}_z + \frac{6(k_{33} - k_{22}) q_c^2 - 2k_{33} + k_{22}}{4(F/\gamma_1)} \tilde{n}_z^2 & \text{in ATC,} \end{cases} \quad (\text{C1})$$

where the numerical constants arise from Galerkin overlap integrals. Since for EC the electric contribution ($\propto \epsilon_a$) is always negligible, the same effects control the value of $\Gamma_3(\mathbf{q})$ in EC and in ATC. Typically, the first term proportional to α_2 (noted hereafter $\Gamma_{3\text{visc}}$) is by far the largest, followed by the elastic contribution ($\Gamma_{3\text{elast}}$). For instance, in EC at $\omega_{\text{CD}} = 0.5$, one has $\{\Gamma_{3\text{visc}}, \Gamma_{3\text{elast}}\} = \{0.84, 0.18\} \Gamma_3(\mathbf{q})$, while at $\omega_{\text{CD}} = 4$, $\{\Gamma_{3\text{visc}}, \Gamma_{3\text{elast}}\} = \{0.66, 0.32\} \Gamma_3(\mathbf{q})$; in ATC, $\{\Gamma_{3\text{visc}}, \Gamma_{3\text{elast}}\} = \{0.91, 0.07\} \Gamma_3(\mathbf{q})$.

There are also contributions of the quadratic nonlinearities to $\Gamma(\mathbf{q})$ (33), which are only important in EC on which

we will now focus. With the use of the quadratic mode $V_2(\mathbf{q}, T)$ (28), which reads

$$V_2(\mathbf{q}, T) = (0, \tilde{n}_y^T S_2(z), 0, 0, \tilde{g}^T S_2(z)) e^{i\mathbf{q} \cdot \mathbf{x}}, \quad (\text{C2})$$

one finds

$$\begin{aligned} \gamma_1 \Gamma_2(\mathbf{q}) = & 2.30 |\alpha_2| q_c^2 \tilde{f} \tilde{n}_y^T + 2 |\alpha_2| q_c \tilde{n}_z \tilde{g}^T - 0.646 \alpha_3 q_c^2 \tilde{f} \tilde{n}_y^T \\ & + (k_{11} - k_{33}) q_c \tilde{n}_z \tilde{n}_y^T, \end{aligned} \quad (\text{C3})$$

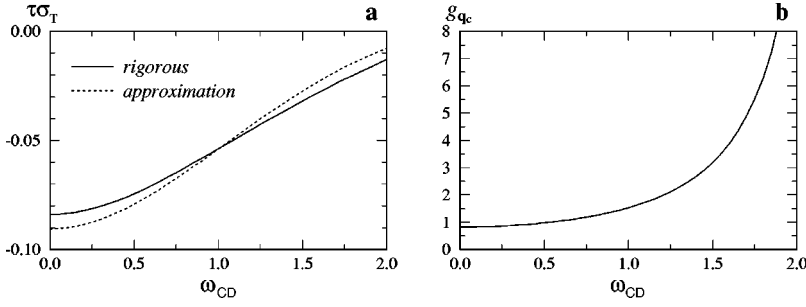


FIG. 10. In EC for MBBA (like Fig. 1): (a) growth rate σ_T of the homogeneous twist mode in units of the characteristic time τ ; (b) saturation coefficient g_{qc} of the critical normal rolls.

where the first two terms dominate. They originate from α_2 terms in $N_{2n_y}(V_1(-\mathbf{q})|V_2(\mathbf{q},T))$, namely $\alpha_2\mathbf{v}\cdot\nabla n_y - \alpha_2(\partial_x v_x)n_y$ for the term $\propto \tilde{n}_y^T$, and $-\alpha_2 n_z(\partial_z v_y)$ for the term $\propto \tilde{g}^T$. The first term in Eq. (C3), $\propto \tilde{n}_y^T$, is always positive. This is due to the fact that $\tilde{n}_y^T > 0$, as can be seen from the result of the adiabatic elimination Eq. (28),

$$\tilde{n}_y^T = [4k_{22} + k_{33}q_c^2]^{-1}(\tilde{n}'_y + |\alpha_2|q_c^2\tilde{g}^T), \quad (\text{C4a})$$

$$\tilde{g}^T = [q_c^2(4\nu_a + \nu_c q_c^2)]^{-1}\tilde{g}', \quad (\text{C4b})$$

where

$$\tilde{n}'_y = (0.323|\alpha_2| - 1.15\alpha_3)q_c^2\tilde{f} + \frac{k_{11} - k_{33}}{2}q_c\tilde{n}_z, \quad (\text{C5a})$$

$$\begin{aligned} \tilde{g}' = & (0.735\alpha_1 + 0.618|\alpha_2| + 0.367\alpha_3 - 0.206\alpha_5 \\ & + 0.367\alpha_6)q_c^4\tilde{f} + 1.22(\alpha_3 + \alpha_6)q_c^2\tilde{f}. \end{aligned} \quad (\text{C5b})$$

In Eq. (C5a), \tilde{n}'_y is dominated by the α_2 contribution originating from the term $\alpha_2(\partial_x v_x)n_y$ in $N_{2n_y}(V_1(\mathbf{q})|V_T)$; in Eq. (C4a), \tilde{n}_y^T is also dominated by this contribution from \tilde{n}'_y . Thus α_2 mechanisms impose the positive value of $\Gamma_2(\mathbf{q})$ (C3).

The increase of $\Gamma_2(\mathbf{q})$ with the frequency ω [Fig. 2(a)] is in fact due to a change of sign of the second term $\propto \tilde{g}^T$ in Eq. (C3). Equation (C5b) gives $\tilde{g}' = (13.2q_c^2 - 28.5)q_c^2\tilde{f}$ which shows that \tilde{g}^T and \tilde{g}' are negative at low ω where q_c is small, and positive at high ω where q_c becomes large. This change of sign is mainly due to the α_2 contribution in Eq. (C5b) originating from the term $\alpha_2\partial_x(v_z\partial_z n_y)$ in $N_{2v_y}(V_1(\mathbf{q})|V_T)$ [62]. It has some consequences on the angle between the projection of the trajectories in the horizontal plane and the axis of the rolls, which could be observed experimentally. In ‘‘zig’’ abnormal or oblique rolls (\mathbf{q}

$= q_c\hat{\mathbf{x}} + p\hat{\mathbf{y}}$ with $p \geq 0$; $\varphi < 0$) one expects according to Eqs. (25), (27) for the component of the velocity parallel to the axis of the rolls [Eq. (B.4) of [29]],

$$v_{\parallel} = 2A|\mathbf{q}|[\tilde{g}(\mathbf{q}) + \varphi\tilde{g}^T(\mathbf{q})]S_2(z)\sin(\mathbf{q}\cdot\mathbf{r}) + \text{h.o.t.}$$

For small p , $\tilde{g}(\mathbf{q}) \approx \tilde{g}_1 p$, and therefore

$$v_{\parallel} \approx 2Aq_c[\tilde{g}_1 p + \varphi\tilde{g}^T(q_c\hat{\mathbf{x}})]S_2(z)\sin(\mathbf{q}\cdot\mathbf{r}). \quad (\text{C6})$$

Since $\tilde{g}_1 > 0$, one has $\tilde{g}_1 p > 0$ in zig oblique rolls, whereas $\varphi\tilde{g}^T(q_c\hat{\mathbf{x}}) < 0$. Thus, when p decreases (this happens spontaneously under certain conditions in EC, see, e.g., [15]), one expects a change of sign of $\arctan(v_{\parallel}/v_{\perp})$, the angle between the trajectories and the wave vector of the rolls [v_{\perp} being the velocity perpendicular to the axis of the rolls, $v_{\perp} \approx -2Aq_c\tilde{f}(q_c\hat{\mathbf{x}})C_1'(z)\sin(\mathbf{q}\cdot\mathbf{r})$ according to Eq. (B.3) of [29]].

APPENDIX D: RESULTS FOR THE ELECTROCONVECTION OF THE NEMATIC MBBA

The (commonly used) nematic MBBA is an interesting example of material without a Lifshitz point. Moreover, in recent experiments the excitation of the twist mode has just been evidenced directly with some special optical methods [17]. For MBBA, the crossover frequency to the dielectric regime is $\omega_D = 2.3\tau_{CD}^{-1}$. We show in Fig. 10 the standard WNL coefficients and in Fig. 11 the predictions of the extended WNL theory concerning the bifurcations of rolls with a normal wave vector. Note that the quadratic effects (Γ_2) determining the value of Γ (33) become dominant at high frequency. Concerning the long-wavelength instabilities, one sees that the standard WNL zig-zag line ϵ_{ZZ}^s is always located above the abnormal-roll line ϵ_{AR} : thus no zig-zag instability would be predicted to occur below the abnormal-roll threshold if the new term Γ_G were not included in Eq. (47c). Within the extended WNL theory, the crossover between the zig-zag and the abnormal-roll instability occurs at

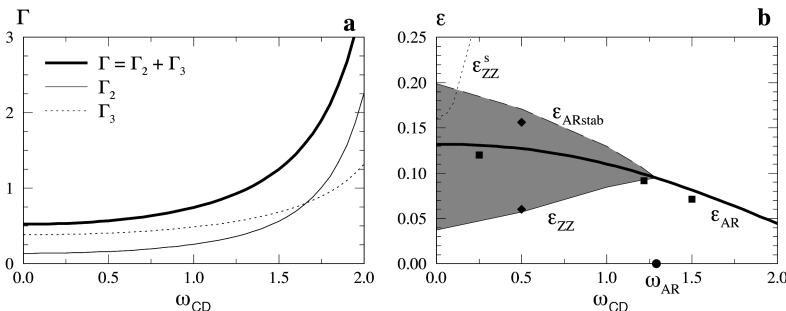


FIG. 11. In EC for MBBA: (a) coupling coefficient $\Gamma(q_c)$ (33) between the critical rolls and the twist mode, as in Fig. 2(a) for N5; (b) stability diagram, as in Fig. 6 for N5. The closed squares and diamonds display the results of the full nonlinear Galerkin computations [3,28].

$\omega_{AR} = 1.3$, with $\epsilon_{AR} \approx 0.095 - 0.058\delta\omega$, $\epsilon_{ARst}/\epsilon_{AR} - 1 \approx -0.41\delta\omega$ or equivalently $\epsilon_{ARst} \approx 0.095 - 0.097\delta\omega$ for $\delta\omega = \omega - \omega_{AR} = O(1)$, with frequencies in units of τ_{CD}^{-1} . Note the good agreement of ϵ_{ARst} with the numerical cal-

culations; this is due to the fact that the amplitudes are smaller in MBBA than in N5. Note also that the bifurcations at zero frequency are similar to those for ATC of 5CB at zero magnetic field.

-
- [1] P.G. de Gennes, *The Physics of Liquid Crystals* (Clarendon Press, Oxford, 1974); S. Chandrasekhar, *Liquid Crystals* (Cambridge University Press, Cambridge, England, 1992).
- [2] E. Dubois-Violette, G. Durand, E. Guyon, P. Manneville, and P. Pieranski, *Solid State Phys., Suppl.* **14**, 147 (1978).
- [3] For a recent review, see A. Buka and L. Kramer, in *Pattern Formation in Liquid Crystals* (Springer-Verlag, New York, 1996).
- [4] W. Helfrich, *J. Chem. Phys.* **51**, 4092 (1969); E. Dubois-Violette, P.G. de Gennes, and O. Parodi, *J. Phys. (France)* **32**, 305 (1971).
- [5] E. Dubois-Violette, *C.R. Acad. Sci.* **273**, 923 (1971); E. Dubois-Violette, E. Guyon, and P. Pieranski, *Mol. Cryst. Liq. Cryst.* **26**, 193 (1973).
- [6] Review articles can be found in I. Rehberg, B.L. Winkler, M. de la Torre, S. Rasenat, and W. Schöpf, *Adv. Solid State Phys.* **29**, 35 (1989); S. Kai and W. Zimmermann, *Prog. Theor. Phys. Suppl.* **99**, 458 (1989); or W. Zimmermann, *MRS Bull.* **XVI**, 46 (1991); L. Kramer and W. Pesch, *Annu. Rev. Fluid Mech.* **27**, 515 (1995).
- [7] E. Bodenschatz, W. Zimmermann, and L. Kramer, *J. Phys. (France)* **49**, 1875 (1988).
- [8] See L.I. Berge, G. Ahlers, and D.S. Cannell, *Phys. Rev. E* **48**, R3236 (1993); and also the contribution of G. Ahlers, in *Pattern Formation in Liquid Crystals* (Ref. [3]).
- [9] M. Treiber and L. Kramer, *Mol. Cryst. Liq. Cryst. Sci. Technol., Sect. A* **261**, 951/311 (1995); M. Dennin, M. Treiber, L. Kramer, G. Ahlers, and D. Cannell, *Phys. Rev. Lett.* **76**, 319 (1996).
- [10] M. Dennin, D.S. Cannell, and G. Ahlers, *Phys. Rev. E* **57**, 638 (1998).
- [11] R. Ribotta, A. Joets, and Lin Lei, *Phys. Rev. Lett.* **56**, 1595 (1986).
- [12] E. Braun, S. Rasenat, and V. Steinberg, *Europhys. Lett.* **15**, 597 (1991).
- [13] S. Nasuno, O. Sasaki, S. Kai, and W. Zimmermann, *Phys. Rev. A* **46**, 4954 (1992).
- [14] E. Plaut and R. Ribotta, *Europhys. Lett.* **38**, 441 (1997).
- [15] E. Plaut, W. Decker, A.G. Rossberg, L. Kramer, W. Pesch, A. Belaidi, and R. Ribotta, *Phys. Rev. Lett.* **79**, 2367 (1997).
- [16] A. Belaidi and R. Ribotta (unpublished).
- [17] S. Rudroff, H. Zhao, L. Kramer, and I. Rehberg, *Phys. Rev. Lett.* **81**, 5144 (1998).
- [18] S. Kai and K. Hirakawa, *Prog. Theor. Phys. Suppl.* **64**, 212 (1978).
- [19] P.H. Bolomey and C. Dimitropoulos, *Mol. Cryst. Liq. Cryst.* **36**, 75 (1976).
- [20] E. Plaut, L. Pastur, and R. Ribotta, *Eur. Phys. J. B* **5**, 283 (1998).
- [21] For an introduction to the order-parameter approach, see, e.g., H. Haken, *Synergetics* (Springer, New York, 1978) or [22] or W. Pesch and L. Kramer, in *Pattern Formation in Liquid Crystals* (Ref. [3]). For examples of applications, see, e.g., M.C. Cross, *Phys. Fluids* **23**, 1727 (1980); M. Bestehorn, R. Friedrich, and H. Haken, *Z. Phys. B* **77**, 151 (1989).
- [22] A.C. Newell, T. Passot, and J. Lega, *Annu. Rev. Fluid Mech.* **25**, 399 (1993).
- [23] Q. Feng, W. Pesch, and L. Kramer, *Phys. Rev. A* **45**, 7242 (1992).
- [24] See, e.g., E. Bodenschatz, W. Pesch, and L. Kramer, *Physica D* **32**, 135 (1988), and references therein.
- [25] M. Kaiser and W. Pesch, *Phys. Rev. E* **48**, 4510 (1993).
- [26] E. Plaut and R. Ribotta, *Phys. Rev. E* **56**, R2375 (1997).
- [27] See the contribution of L. Kramer and W. Pesch, in *Pattern Formation in Liquid Crystals* (Ref. [3]).
- [28] W. Decker, Ph.D. thesis, University of Bayreuth, 1995.
- [29] E. Plaut and R. Ribotta, *Eur. Phys. J. B* **5**, 265 (1998).
- [30] See A.G. Rossberg, A. Hertrich, L. Kramer, and W. Pesch, *Phys. Rev. Lett.* **76**, 4729 (1996); A.G. Rossberg and L. Kramer, *Phys. Scr.* **67**, 121 (1996); A.G. Rossberg, Ph.D. thesis, University of Bayreuth, 1998.
- [31] R.M. Clever and F.H. Busse, *J. Fluid Mech.* **65**, 625 (1974).
- [32] S. Chandrasekhar, *Hydrodynamic and Hydromagnetic Stability* (Clarendon Press, Oxford, 1961).
- [33] For EC see, e.g., [27] and M. Treiber, Ph.D. thesis, University of Bayreuth, 1996; for ATC see, e.g., [23], which was later corrected in [29].
- [34] The linear expansion in ϵ (20) can be used for roll modes with any wave vector \mathbf{q} . However, in EC for nematics with $\epsilon_a < 0$ and in the region $q \ll q_c$, no neutral roll modes exist [7], i.e., $\epsilon_0(\mathbf{q})$ and τ_q become negative and no longer correspond to a threshold and a characteristic time, respectively.
- [35] There exist also *parallel rolls* of wave vector \mathbf{q} parallel to $\hat{\mathbf{y}}$ [8,23], but, in the director-dominated regime, their growth rates are very negative as compared with the growth rate of the critical roll mode, i.e., they are totally damped out.
- [36] More generally the active modes are the modes with which one can capture the macroscopic dynamics of the system [22]. It is only in the WNL regime that they can safely be identified with linear modes of not too negative growth rates.
- [37] This can be understood by the fact that all equations contain diffusion terms. Thus $\sigma_m(\mathbf{q}; R)$ is typically of the form $\sigma_m(\mathbf{0}; R) - \nu_h \mathbf{q}^2$, where ν_h is a horizontal diffusivity and $\sigma_m(\mathbf{0}; R)$ is due to the vertical diffusion.
- [38] In contrast to the twist mode which is of the symmetry type — with respect to the reflection $z \mapsto -z$, the splay mode is of the symmetry type +. Since the rule (17) imposes $\text{sym}[N_2(V_1(\mathbf{q}; R), V_1(-\mathbf{q}; R))] = -1$, the splay mode does not couple with the rolls at quadratic order. But, according to the same rule, $\text{sym}[N_3(V_1(\mathbf{q}; R), V_1(-\mathbf{q}; R), V_5)] = +1$: the splay mode could possibly be excited at cubic order by coupling with two roll modes.
- [39] At $z=0$, $S_1(z)=1$. For oblique rolls, Eq. (39) is in fact also valid since the n_y contributions of order A are odd and vanish

- at $z=0$. Note also that generally the in-plane director averaged over the thickness of the layer is $\hat{\mathbf{x}}+2/\pi\varphi\hat{\mathbf{y}}+\text{h.o.t.}$
- [40] The solutions (37) then become unphysical since $(1+b_{\mathbf{q}})\beta_3(\mathbf{q})<0$.
- [41] In these anomalous oblique rolls one could have $p\varphi>0$, in contrast to the ‘‘standard’’ oblique rolls where $p\varphi<0$.
- [42] Additional time-derivative terms in the mean-flow equation are generated by the contributions $\alpha_2\dot{\mathbf{n}}\otimes\mathbf{n}+\alpha_3\mathbf{n}\otimes\dot{\mathbf{n}}$ to the viscous stress tensor. We will not consider these terms since we focus only on the *marginal stability* of rolls.
- [43] The twist contribution $2b_1\gamma'/\sigma_T$ in Eq. (49) was absorbed in the contributions a_7-a_8 in Eq. (45) of [25].
- [44] The mechanism (M2) becomes even clearer if the quadratic source terms for φ in Eq. (47b) are reformulated by insertion of $A=|A|e^{i\mathbf{q}\cdot\mathbf{r}}$ where \mathbf{q} is the local wave vector of the rolls (the gradient of the phase of the rolls). One then obtains $i\gamma'(A^*\partial_y A-A\partial_y A^*)=-2\gamma'|A|^2q_y$ which shows clearly the repulsive torque between the oblique component of the roll wave vector and the in-plane director.
- [45] The difference of signs with [25] is due to the fact that our Poisseulle profile $P_1(z)$ is now positive for $-\pi/2<z<\pi/2$.
- [46] The ratio of the zig-zag threshold with, Eq. (52a), and without, Eq. (53), the Γ_φ effects decreases with the frequency in EC: this ratio tends to 1 when $\omega\rightarrow\omega_L^+$, and reaches 0.73 at $\omega_{\text{CD}}=3$. Thus, whereas the Γ_φ effects are not crucial for the zig-zag instability, they control the precise value of the corresponding threshold at high frequency.
- [47] The relation between the slopes of ϵ_{ZZ} and ϵ_{AR} at the crossover point was found from a simpler phase-diffusion model by H. Zhao and L. Kramer (private communication); see also [17].
- [48] The coefficients determining the bimodal growth rate (61) are then $\epsilon_0(\mathbf{k})=2.02$, $\tau_{\mathbf{k}}=12.5=6.4\tau_{\mathbf{q}}$, $\beta_2(\mathbf{k})=-0.33$, $\beta_3(\mathbf{k})=-0.11$, $g_{\mathbf{qk}}=-0.21$; at $\epsilon=\epsilon_{\text{BV}}(\mathbf{q})=0.14$, one has $A(\mathbf{q};\epsilon)=0.27$ and $\varphi(\mathbf{q};\epsilon)=-0.37$.
- [49] The coefficients are now $\epsilon_0(\mathbf{k})=0.29$, $\tau_{\mathbf{k}}=2.1=1.8\tau_{\mathbf{q}}$, $\beta_2(\mathbf{k})=-0.42$, $\beta_3(\mathbf{k})=0.36$, $g_{\mathbf{qk}}=1.36$; and $\epsilon=\epsilon_{\text{BV}}(\mathbf{q})=0.186A(\mathbf{q};\epsilon)=0.23$, and $\varphi(\mathbf{q};\epsilon)=-0.45$.
- [50] In Ref. [10] the name ‘‘SO2’’ was used for the bimodal-varicose structure. Using parameters taken from [9,10] (with changes of less than 10% to fit the wave vector of the oblique rolls at threshold) we reconstruct, e.g., the sequence of Fig. 12 of [10] with values of ϵ_{BV} and $\arg\mathbf{k}$ which differ less than 25% from the experimental ones.
- [51] In EC at low ω , the contributions of $\beta_3(\mathbf{k})$ or $g_{\mathbf{qk}}$ in Eq. (61) can also become positive for the duals found very far from \mathbf{q}_c , but these contributions are still dominated by the $\beta_2(\mathbf{k})$ contribution in Eq. (61).
- [52] When $\mathbf{k}=k_x\hat{\mathbf{x}}+k_y\hat{\mathbf{y}}\mapsto S(\mathbf{k})=k_x\hat{\mathbf{x}}-k_y\hat{\mathbf{y}}$, the fields θ, n_z , and f are not changed in $V_1(\mathbf{k})$, whereas the fields n_y and g are changed into their opposite. But, since these fields play only a secondary role in the convection mechanism, they are always of smaller magnitude than the other ones in the linear mode $V_1(\mathbf{k})$. Therefore this change of sign in n_y and g is only a second-order effect in $V_1(\mathbf{k})$, and consequently the second harmonics $V_2(\mathbf{q},\mathbf{k})$ and $V_2(-\mathbf{q},\mathbf{k})$ are only slightly modified. Finally $g_{\mathbf{qk}}$ (59) is roughly unchanged: $g_{\mathbf{qS}(\mathbf{k})}\simeq g_{\mathbf{qk}}$.
- [53] For EC, see [19] and [18] where the symmetric bimodals and oscillating bimodals were named, respectively, ‘‘grid pattern’’ and ‘‘oscillating grid pattern’’; or A. Joets and R. Ribotta, J. Phys. (France) **47**, 595 (1986). For ATC, see [20].
- [54] H. Riecke, Phys. Rev. Lett. **68**, 301 (1992).
- [55] See [10] and H. Riecke and G.D. Granzow, Phys. Rev. Lett. **81**, 333 (1998).
- [56] See, e.g., the experimental work of A. Belaidi, Ph.D. thesis, University of Orsay, 1998; or the comparison between experiments and a coupled phase-diffusion equations model in [17].
- [57] See, e.g., B. Jانياud, H. Kokubo, and M. Sano, Phys. Rev. E **47**, R2237 (1993), and references therein.
- [58] H. Richter, A. Buka, and I. Rehberg, in *Spatio-Temporal Patterns in Nonequilibrium Complex Systems*, edited by P. E. Cladis and P. Palfy-Muhoray (Addison-Wesley Publishing Company, Reading, MA, 1994).
- [59] An important difference is that the Goldstone mode can be excited immediately at threshold; this has been shown in [30] to lead to a new type of spatiotemporal chaos. Also, in [30] the rotational invariance imposes some constraints on the nonlinearities which reduce the number of independent coefficients in the amplitude equations.
- [60] A. Hertrich, Ph.D. thesis, University of Bayreuth, 1996.
- [61] J.-H. Huh, Y. Hidaka, and S. Kai, Phys. Rev. E **58**, 7355 (1998).
- [62] This is a contribution of the term $\alpha_2\dot{\mathbf{n}}\otimes\mathbf{n}=\alpha_2(\mathbf{v}\cdot\nabla\mathbf{n})\otimes\mathbf{n}$ in the viscous stress tensor, where $\dot{\mathbf{n}}$ reduces to its advection part for stationary solutions. It indicates that a rotation of the director in the horizontal plane ($\dot{\mathbf{n}}\cdot\hat{\mathbf{y}}\neq 0$) feeds back on the flow and creates a v_y or g mode in $S_2(z)e^{iqx}$.